NUREG/CR-1274
ORNL/NUREG/TM-369
Dist. Category RF

Contract No. W-7405-eng-26

Engineering Technology Division

FLAW PREPARATIONS FOR HSST PROGRAM VESSEL FRACTURE MECHANICS TESTING: MECHANICAL-CYCLIC PUMPING AND ELECTRON-BEAM WELD-HYDROGEN-CHARGE CRACKING SCHEMES

P. P. Holz

Manuscript Completed-April 29, 1980
Date Published-May 1980

NOTICE This document contains information of a preliminary nature. It is subject to revision or correction and therefore does not represent a final report.

Prepared for the U.S. Nuclear Regulatory Commission
Office of Nuclear Regulatory Research
Under Interagency Agreements DOE 40-551-75 and 40-552-75

NRC FIN No. B0119

Prepared by the
OAK RIDGE NATIONAL LABORATORY
Oak Ridge, Tennessee 37830
operated by
UNION CARBIDE CORPORATION
for the
DEPARTMENT OF ENERGY

CONTENTS

PREFACE

The work reported here was performed at Oak Ridge National Laboratory (ORNL) under sponsorship of the U.S. Nuclear Regulatory Commission's (NRC's) Heavy-Section Steel Technology Program, which is directed by ORNL. The program is conducted as part of the ORNL Pressure Vessel Technology Program, of which G. D. Whitman is manager. The manager for the NRC is Milton Vagins.

This report is designated Heavy-Section Steel Technology Program Technical Report 57. Prior reports in this series are listed below:

1. S. Yukawa, *Evaluation of Periodic Proof Testing and Warm Prestressing Procedures for Nuclear Reactor Vessels*, HSSTP-TR-1, General Electric Company, Schenectady, N.Y. (July 1, 1969).
2. L. W. Loechel, *The Effect of Section Size on the Transition Temperature in Steel*, MCR-69-189, Martin Marietta Corporation, Denver, Colo. (Nov. 20, 1969).
3. P. N. Randall, *Gross Strain Measure of Fracture Toughness of Steels*, HSSTP-TR-3, TRW Systems Group, Redondo Beach, Calif. (Nov. 1, 1969).
4. C. Visser, S. E. Gabrielse, and W. VanBuren, *A Two-Dimensional Elastic-Plastic Analysis of Fracture Test Specimens*, WCAP-7368, Westinghouse Electric Corporation, PWR Systems Division, Pittsburgh, Pa. (October 1969).
5. T. R. Mager, F. O. Thomas, and W. S. Hazelton, *Evaluation by Linear Elastic Fracture Mechanics of Radiation Damage to Pressure Vessel Steels*, WCAP-7328 (Rev.), Westinghouse Electric Corporation, PWR Systems Division, Pittsburgh, Pa. (October 1969).
6. W. O. Shabbits, W. H. Pryle, and E. T. Wessel, *Heavy Section Fracture Toughness Properties of A533 Grade B Class 1 Steel Plate and Submerged Arc Weldment*, WCAP-7414, Westinghouse Electric Corporation, PWR Systems Division, Pittsburgh, Pa. (December 1969).
7. F. J. Loss, *Dynamic Tear Test Investigations of the Fracture Toughness of Thick-Section Steel*, NRL-7056, U.S. Naval Research Laboratory, Washington, D.C. (May 14, 1970).
8. P. B. Crosley and E. J. Ripling, *Crack Arrest Fracture Toughness of A533 Grade B Class 1 Pressure Vessel Steel*, HSSTP-TR-8, Materials Research Laboratory, Inc., Glenwood, Ill. (March 1970).
9. T. R. Mager, *Post-Irradiation Testing of 2T Compact Tension Specimens*, WCAP-7561, Westinghouse Electric Corporation, PWR Systems Division, Pittsburgh, Pa. (August 1970).
10. T. R. Mager, *Fracture Toughness Characterization Study of A533, Grade B, Class 1 Steel*, WCAP-7578, Westinghouse Electric Corporation, PWR Systems Division, Pittsburgh, Pa. (October 1970).
11. T. R. Mager, *Notch Preparation in Compact Tension Specimens*, WCAP-7579, Westinghouse Electric Corporation, PWR Systems Division, Pittsburgh, Pa. (November 1970).
12. N. Levy and P. V. Marcal, *Three-Dimensional Elastic-Plastic Stress and Strain Analysis for Fracture Mechanics, Phase I: Simple Flawed Specimens*, HSSTP-TR-12, Brown University, Providence, R.I. (December 1970).
13. W. O. Shabbits, *Dynamic Fracture Toughness Properties of Heavy Section A533 Grade B, Class 1 Steel Plate*, WCAP-7623, Westinghouse Electric Corporation, PWR Systems Division, Pittsburgh, Pa. (December 1970).
14. P. N. Randall, *Gross Strain Crack Tolerance of A533-B Steel*, HSSTP-TR-14, TRW Systems Group, Redondo Beach, Calif. (May 1, 1971).

15. H. T. Corten and R. H. Sailors, *Relationship Between Material Fracture Toughness Using Fracture Mechanics and Transition Temperature Tests*, T&AM Report 346, University of Illinois, Urbana, Ill. (Aug. 1, 1971).

16. T. R. Mager and V. J. McLoughlin, *The Effect of an Environment of High Temperature Primary Grade Nuclear Reactor Water on the Fatigue Crack Growth Characteristics of A533 Grade B Class 1 Plate and Weldment Material*, WCAP-7776, Westinghouse Electric Corporation, PWR Systems Division, Pittsburgh, Pa. (October 1971).

17. N. Levy and P. V. Marcal, *Three-Dimensional Elastic-Plastic Stress and Strain Analysis for Fracture Mechanics, Phase II: Improved Modeling*, HSSTP-TR-17, Brown University, Providence, R.I. (November 1971).

18. S. C. Grigory, *Six-inch-thick Flawed Tensile Tests, First Technical Summary Report, Longitudinal Specimens 1 through 7*, HSSTP-TR-18, Southwest Research Institute, San Antonio, Tex. (June 1972).

19. P. N. Randall, *Effects of Strain Gradients on the Gross Strain Crack Tolerance of A533-B Steel*, HSSTP-TR-19, TRW Systems Group, Redondo Beach, Calif. (May 1, 1972).

20. S. C. Grigory, *Tests of Six-inch-thick Flawed Tensile Specimens, Second Technical Summary Report, Transverse Specimens Numbers 8 through 10, Welded Specimens Numbers 11 through 13*, HSSTP-TR-20, Southwest Research Institute, San Antonio, Tex. (June 1972).

21. L. A. James and J. A. Williams, *Heavy-Section Steel Technology Program Technical Report No. 21, The Effect of Temperature and Neutron Irradiation upon the Fatigue-Crack Propagation Behavior of ASTM A533, Grade B, Class 1 Steel*, HEDL-TME-72-132, Hanford Engineering Development Laboratory, Richland, Wash. (September 1972).

22. S. C. Grigory, *Tests of Six-inch-thick Flawed Tensile Specimens, Third Technical Summary Report, Longitudinal Specimens Numbers 14 through 16, Unflawed Specimen Number 17*, HSSTP-TR-22, Southwest Research Institute, San Antonio, Tex. (October 1972).

23. S. C. Grigory, *Tests of Six-inch-thick Flawed Tensile Specimens, Fourth Technical Summary Report, Tests of One-inch-thick Flawed Tensile Specimens for Size Effect Evaluation*, HSSTP-TR-23, Southwest Research Institute, San Antonio, Tex. (June 1973).

24. S. P. Ying and S. C. Grigory, *Tests of Six-inch-thick Tensile Specimens, Fifth Technical Summary Report, Acoustic Emission Monitoring of One-inch and Six-inch-thick Tensile Specimens*, HSSTP-TR-24, Southwest Research Institute, San Antonio, Tex. (November 1972).

25. R. W. Derby et al., *Test of 6-inch-thick Pressure Vessels. Series 1: Intermediate Test Vessels V-1 and V-2*, ORNL-4895 (February 1974).

26. W. J. Stelzman and R. G. Berggren, *Radiation Strengthening and Embrittlement in Heavy Section Plates and Welds*, ORNL-4871 (June 1973).

27. P. B. Crosley and E. J. Ripling, *Crack Arrest in an Increasing K-Field*, HSSTP-TR-27, Materials Research Laboratory, Glenwood, Ill. (January 1973).

28. P. V. Marcal, P. M. Stuart, and R. S. Bettes, *Elastic-Plastic Behavior of a Longitudinal Semi-Elliptical Crack in a Thick Pressure Vessel*, Brown University, Providence, R.I. (June 1973).

29. W. J. Stelzman, *Characterization of HSST Plates 01, 02, and 03* (in preparation).

30. D. A. Canonico, *Characterization of Heavy Section Weldments in Pressure Vessel Steels* (in preparation).

31. J. A. Williams, *The Irradiation and Temperature Dependence of Tensile and Fracture Properties of ASTM A533, Grade B, Class 1 Steel Plate and Weldment*, HEDL-TME 73-75, Hanford Engineering Development Laboratory, Richland, Wash. (August 1973).

32. J. M. Steichen and J. A. Williams, *High Strain Rate Tensile Properties of Irradiated ASTM A533 Grade B Class 1 Pressure Vessel Steel*, HEDL-TME 73–74, Hanford Engineering Development Laboratory, Richland, Wash. (July 1973).
33. P. C. Riccardella and J. L. Swedlow, *A Combined Analytical-Experimental Fracture Study*, WCAP-8224, Westinghouse Electric Corporation, PWR Systems Division, Pittsburgh, Pa. (October 1973).
34. R. J. Podlasek and R. J. Eiber, *Final Report on Investigation of Mode III Crack Extension in Reactor Piping*, Battelle Columbus Laboratories, Columbus, Ohio (May 1974).
35. T. R. Mager et al., *Interim Report on the Effect of Low Frequencies on the Fatigue Crack Growth Characteristics of A533 Grade B Class 1 Plate in an Environment of High-Temperature Primary Grade Nuclear Reactor Water*, WCAP-8256, Westinghouse Electric Corporation, Pittsburgh, Pa. (December 1973).
36. J. A. Williams, *The Irradiated Fracture Toughness of ASTM A533, Grade B, Class 1 Steel Measured with a Four-inch-thick Compact Tension Specimen*, HEDL-TME 75–10, Hanford Engineering Development Laboratory, Richland, Wash. (January 1975).
37. R. H. Bryan et al., *Test of 6-in.-thick Pressure Vessels, Series 2: Intermediate Test Vessels V-3, V-4, and V-6*, ORNL-5059 (November 1975).
38. T. R. Mager, S. E. Yanichko, and L. R. Singer, *Fracture Toughness Characterization of HSST Intermediate Pressure Vessel Material*, WCAP-8456, Westinghouse Electric Corporation, Pittsburgh, Pa. (December 1974).
39. J. G. Merkle, G. D. Whitman, and R. H. Bryan, *An Evaluation of the HSST Program Intermediate Pressure Vessel Tests in Terms of Light-Water Reactor Pressure Vessel Safety*, ORNL/TM-5090 (November 1975).
40. J. G. Merkle et al., *Test of 6-in.-thick Pressure Vessels, Series 3: Intermediate Test Vessel V-7*, ORNL/NUREG-1 (August 1976).
41. J. A. Davidson et al., *The Irradiated Dynamic Fracture Toughness of ASTM A533, Grade B, Class 1 Steel Plate and Submerged-Arc Weldment*, WCAP-8775, Westinghouse Electric Corp., Pittsburgh, Pa. (October 1976).
42. R. D. Cheverton, *Pressure Vessel Fracture Studies Pertaining to a PWR LOCA-ECC Thermal Shock: Experiments TSE-1 and TSE-2*, ORNL/NUREG/TM-3 (September 1976).
43. J. G. Merkle et al., *Test of 6-inch-thick Pressure Vessels. Series 4: Intermediate Test Vessels V-5 and V-9*, ORNL/NUREG-7 (August 1977).
44. J. A. Williams, *The Ductile Fracture Toughness of Heavy Section Steel Plate*, Hanford Engineering Development Laboratory, Richland, Wash. (September 1979).
45. R. H. Bryan et al., *Test of 6-in.-thick Pressure Vessels. Series 3: Intermediate Test Vessel V-7A under Sustained Loading*, ORNL/NUREG-9 (February 1978).
46. R. D. Cheverton and S. E. Bolt, *Pressure Vessel Fracture Studies Pertaining to a PWR LOCA-ECC Thermal Shock: Experiments TSE-3 and TSE-4, and Update of TSE-1 and TSE-2 Analysis*, ORNL/NUREG-22 (December 1977).
47. D. A. Canonico, *Significance of Reheat Cracks to the Integrity of Pressure Vessels for Light-Water Reactors*, ORNL/NUREG-15 (July 1977).
48. G. C. Smith and P. P. Holz, *Repair Weld Induced Residual Stresses in Thick-Walled Steel Pressure Vessels*, NUREG/CR-0093 (ORNL/NUREG/TM-153) (June 1978).

49. P. P. Holz and S. W. Wismer, *Half-Bead (Temper) Repair Welding for Heavy-Section Steel Technology Vessels*, NUREG/CR-0113 (ORNL/NUREG/TM-177) (June 1978).

50. G. C. Smith, P. P. Holz, and W. J. Stelzman, *Crack Extension and Arrest Tests of Axially Flawed Steel Model Pressure Vessels*, NUREG/CR-0126 (ORNL/NUREG/TM-196) (in preparation).

51. R. H. Bryan et al., *Test of 6-in.-Thick Pressure Vessels. Series 3: Intermediate Test Vessel V-7B*, NUREG/CR-0309 (ORNL/NUREG-38) (October 1978).

52. R. D. Cheverton, S. K. Iskander, and S. E. Bolt, *Applicability of LEFM to the Analysis of PWR Vessels Under LOCA-ECC Thermal Shock Conditions*, NUREG/CR-0107 (ORNL/NUREG-40) (October 1978).

53. R. H. Bryan et al., *Test of 6-in.-Thick Pressure Vessels. Series 3: Intermediate Test Vessel V-8*, NUREG/CR-0675 (ORNL/NUREG-58) (December 1979).

54. R. D. Cheverton, *Application of Static and Dynamic Crack Arrest Theory to TSE-4*, NUREG/CR-0767 (ORNL/NUREG-57) (June 1979).

55. J. A. Williams, *Tensile Properties of Irradiated and Unirradiated Welds of A533 Steel Plate and A508 Forgings*, NUREG/CR-1158 (ORNL/Sub-79-50917/2), Handford Engineering Development Laboratory, Richland, Wash. (July 1979).

56. K. W. Carlson and J. A. Williams, *The Effect of Crack Length and Side Groove on the Ductile Fracture Toughness Properties of ASTM A533 Steel*, NUREG/CR-1171 (ORNL/Sub-79/50917/3) Hanford Engineering Development Laboratory, Richland, Wash. (October 1979).

ACKNOWLEDGMENTS

The author acknowledges with gratitude the many contributions by his Section Head, G. D. Whitman; his colleagues R. H. Bryan, R. D. Cheverton, J. G. Merkle, and G. C. Robinson; and senior technicians H. D. Curtis and Tom King, Jr. Thanks also go to Jim Murphy and S. A. Wallace of the Y-12 Development Division, J. D. Hudson of ORNL's Metals and Ceramics Division, K. K. Klindt of ORNL's Quality Assurance and Inspection Division, Hubert Felix and R. A. Huber of the Y-12 Assembly-Welding Group, P. S. Ashburn of the Y-12 Electrical Maintenance Department, and Y-12's Building 9201-1 Main Machine Shop personnel under direction of C. E. Bolyard and W. F. Cartwright for excellent assistance in their respective fields. And finally, a thank you is also given to many others, unlisted herein, for day-to-day cooperation and assistance.

Flaw Preparations for HSST Program Vessel Fracture Mechanics Testing: Mechanical-Cyclic Pumping and Electron-Beam Weld-Hydrogen-Charge Cracking Schemes

P. P. Holz

ABSTRACT

Representative field testing to determine data for potential flaw propagation, fracture behavior, and margin against fracture for high-pressure-, high-temperature-service steel vessels subjected to increasing pressurization and/or thermal shock is premised on the investigators' ability to grow representative sharp cracks of known size, location, and orientation. Gaging for analytical stress and strain procedures and ultrasonic and acoustic emission instrumentation can then be applied to monitor the vessel during testing and to study crack growth.

Cracks were grown by two techniques: (1) a mechanical method wherein a premachined notch was sharpened by pressurization and (2) a method combining electron-beam welds and hydrogen charging to crack the chill zone of a rapidly placed autogenous weld. The mechanical method produces a naturally occurring growth shape controlled primarily by the shape of the machined notch; the welding-electrochemical method produces flaws of uniform depth from the surface of a wall or machined notch.

Theories, details, discussions, and procedures are covered for both of the flaw-growing schemes.

1. INTRODUCTION

The Heavy-Section Steel Technology (HSST) Program is an engineering investigation of the structural behavior in the presence of flaws and inhomogeneities of thick pressure vessels typical of current and future water-cooled reactors under startup, operating, accident, and cooldown conditions. Extensive testing programs are under way for determining the fracture behavior and margin against fracture on approximately one-fourth-scale diameter reactor pressure vessels of 15.24-cm (6-in.) wall thickness fabricated with typical steels. For the tests, the preflawed vessels are instrumented extensively, including acoustic emission (AE) sensing and, where possible, ultrasonic (UT) monitoring. Then they are subjected to increasing hydrostatic or pneumatic pressurization until burst or leakage occurs. Similar tests are also conducted on vessel cylinder sections of the same size to investigate the potential for flaw propagation in pressurized-water reactor (PWR) vessels during injection of emergency core coolant following a loss-of-coolant accident. Results from these efforts serve the needs of the regulatory and safety bodies, the professional code-writing bodies, and the nuclear power industry.

One phase of the investigation in the HSST Program requires that sharp cracks of known size, location, and orientation be grown in the walls of massive steel test specimens and vessels to simulate naturally occurring flaws. The flaw must be characterized properly for the application of fracture mechanics analysis. During the experiment, flaw growth evaluation can then be determined within the capabilities of UT and AE techniques. Sharp cracks are required for all test temperatures to simulate naturally occurring defects properly and conservatively.

Cracks were grown by two techniques. One, based on mechanical techniques, involves the use of high-pressure pulsating fluids to fatigue a machined notch placed in the structure. In this technique, sharp flaws are produced by cyclic notch pressurization applied by high-pressure hydraulic pumping equipment. The other method, based on metallurgical principles, involves the combination of electron-beam (EB) or laser-beam welding with an electrochemical process to crack the weld by hydrogen charging. Long flaws of uniform depth can be produced by the welding method, whereas mechanically produced flaws tend to exhibit contours controlled by the initial machined notch.

2. BACKGROUND

In our earliest tensile tests of 15.24-cm-thick (6-in.) specimens at Southwest Research Institute, an attempt was made to (1) machine semielliptical notches using the electric discharge machining (EDM) process and (2) develop stress-corrosion procedures to initiate sharp cracks at the root of an EDM notch. The procedure used ammonium nitrate (NH_4NO_3) to induce stress-corrosion cracking as a technique to produce the flaw.[1] Ammonium nitrate was poured into the notch while the specimen was maintained at 121° C (250° F) under static load. This attempt failed because the cracks, although sharp, were also branched severely, causing a loss of constraint. The static load required to generate the crack was too great; that is, yielding at the tip of the crack at the temperature at which the crack was generated affected the load required to cause specimen failure in the transition temperature range and lower.

Subsequently, most of the flaws for tensile tests and the following vessel tests were fatigue sharpened by hydraulically pulsing a part-circular or semielliptical machined void with the apparatus shown in Figs. 1 and 2. For cyclic pumping, the machined notch is filled with hydraulic oil, and the opening sealed with a rubber O-ring and a clamping device. The notch cavity connects to the pumping system through the clamping device. For cyclic pump loading, in effect, the hydraulic oil acts like a wedge that is pushed into the notch and then removed.

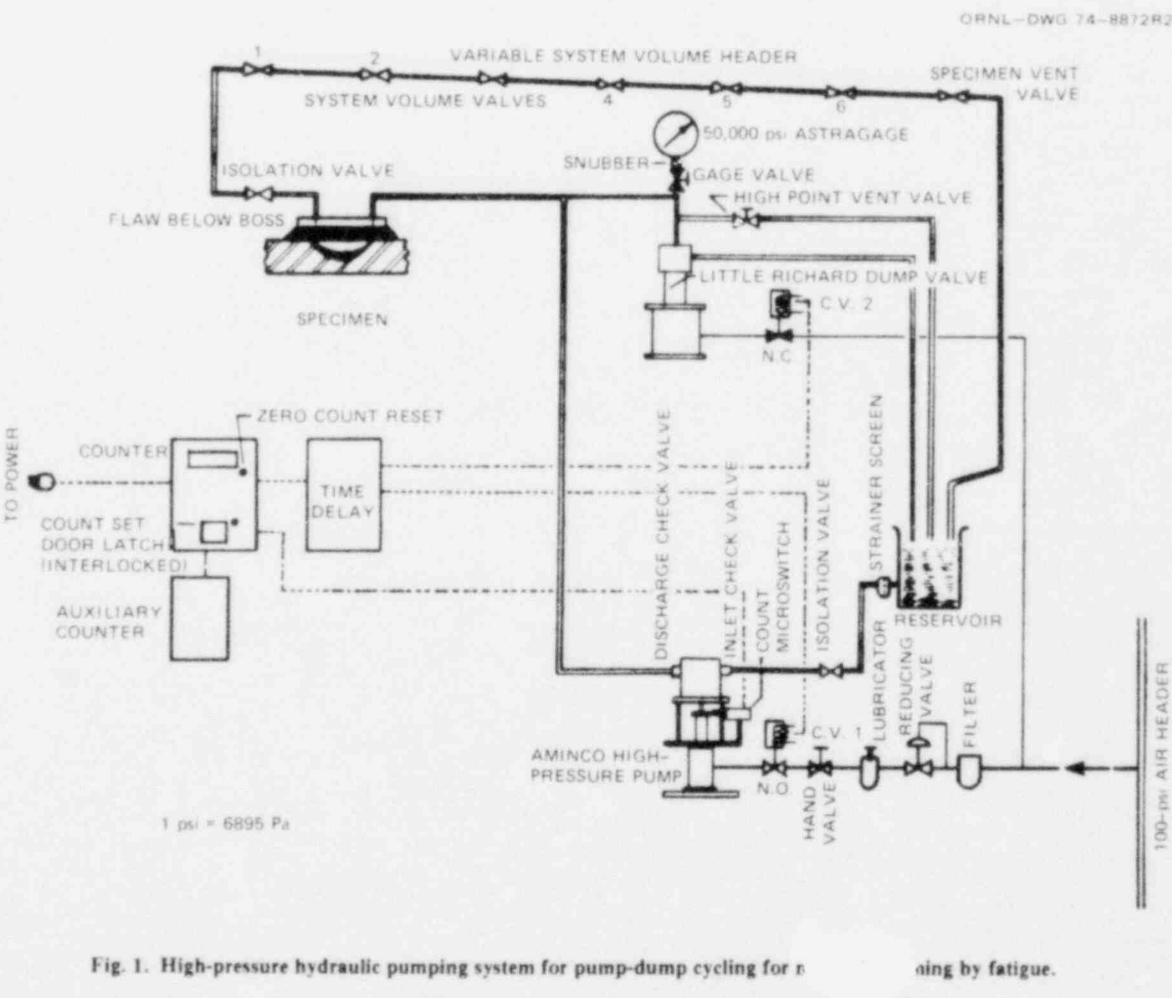

Fig. 1. High-pressure hydraulic pumping system for pump-dump cycling for r [illegible] ning by fatigue.

ORNL-DWG 80-4260 ETD

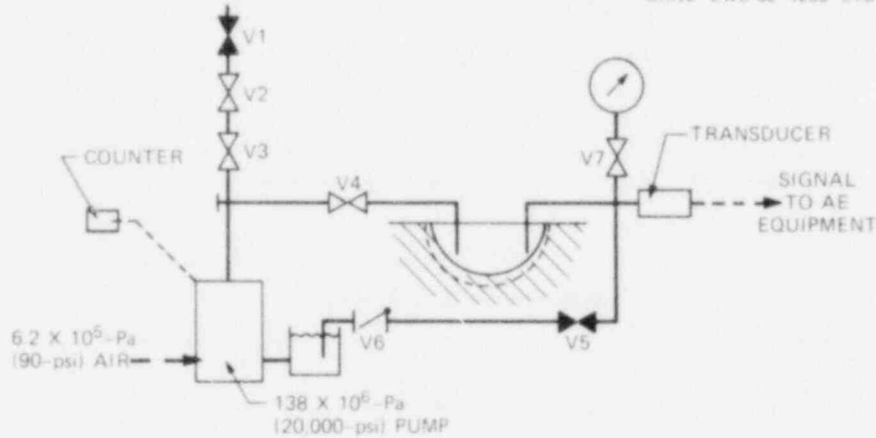

Fig. 2. Direct fatigue-pump cycling system.

For the straight pumping arrangement (Fig. 2), each stroke of the hydraulic pump pressurizes the machined void and a parallel adjusted volume simultaneously, permitting control of the pressure level and stress-intensity range desired. The alternate pump-dump arrangement (Fig. 1) is used when more than one stroke of the hydraulic pump is required to obtain sufficient pressure, and a dump valve is required to obtain cutoff at the precise pressure level. Both pulsing techniques were used in the flaw sharpening of most of the intermediate pressure vessels, including inside nozzle corner applications, where the flaw shape was specifically chosen so that most of the crack front would grow in a nearly uniform manner under cyclic pressure. However, the extension of these pumping procedures to other crack shapes, such as long surface cracks, is extremely difficult because pumped crack fronts tend to grow nonuniformly. A long notch also presents sealing problems for effective pumping. Furthermore, the pumping equipment presently available for cyclically pressurizing large flaws is inadequate because of volume requirement. The acquisition of additional equipment would have entailed long-term delays and expensive pump development.

The combination of EB welding and electrochemical hydrogen charging is not limited by the length of the flaw and is capable of producing uniform, sharp cracks for all machinable shapes. This method was selected for the three tests in the vessel V-7 series and for thermal shock test cylinders. Following a concentrated development effort, it provided the means to successfully produce the sharp crack in the vessel or test cylinders.

3. MECHANICAL FLAWING METHOD

3.1 General

In the mechanical method of sharpening flaws for a test specimen, a suitable slot is machined into the vessel wall, a mold replication of the machined notch is made for templating shim stock to conform dimensionally to the notch, and the shim stock is inserted to fill the entire notch volume except for the contact surface contour line at the root of the notch. The notch is then sealed by a block welded or clamped to the test specimen, and the volume to be pressurized cyclically is connected to a pressurizing system. Figure 1 illustrates the schematics of a high-pressure hydraulic pumping system for pump-dump cycling up to 193 MPa (28,000 psi) at 50 to 52 strokes per minute. Figure 2 is a schematic version of the simplified high-pressure hydraulic pumping system for direct fatigue-pump cycling up to 114 MPa (16,500 psi) at 30 to 35 strokes per minute.

For sharpening the notch, a notch of the approximate shape of the desired crack first is sealed carefully and then is filled with the oil through a small access opening. Thereafter, to fatigue the notch and grow the crack, the oil in the notch is pressurized repeatedly.

An estimated cyclic pressure required to grow the flaw can be determined by the desired stress-intensity factor at the tip of the fatigue-growing crack according to the equation $\Delta p = \Delta K_I / C\sqrt{\pi a}$, where C is the fracture mechanics shape factor for uniform stress. For example, a cyclic pressure or nominal stress Δp of 138 MPa (20,000 psi) is required for a flaw with a desired stress-intensity factor ΔK_I of 49.6 $MN \cdot m^{-3/2}$ (45,000 psi$\sqrt{in.}$), a notch center depth defect (generally half length) a of 0.0508 m (2 in.), and a calculated value C of 0.9.

Methods exist to estimate the number of load cycles required to sharpen a machined notch by fatigue and thereby grow a flaw to predetermined depth. The sharpening of a machined notch by fatigue takes place in three phases: (1) the initiation of a fatigue flaw at the base of the machined notch; (2) a delay in the growth of the flaw due to a reduction in the cyclic load level, if any; and (3) the growth of the flaw due to a reduction in the cyclic load level, if any; and (3) the growth of the flaw by fatigue under cyclic load. Paul Paris's fatigue crack growth method is available to calculate the number of load cycles corresponding to phases (2) and (3) (ref. 2). The calculation is based on the fracture mechanics approach described by the equation $da/dN = C_f(\Delta K_I)^n$, where da/dN is the crack growth rate, K_I is the stress-intensity factor, and C_f and n are constants to be determined by test. Crack initiation at the base of the machined notch, however, appears to depend on a number of geometric variables, including the notch root radius, plasticity of the material, and proximate volume conformity of the shim insert block to the void volume of the premachined notch. Even applying the considerable experimental fatigue-pump data from our work to arrive at a prediction number for crack initiation cycling requirements is difficult. Cumulative results from a number of cycles vary greatly from prototype mock-ups to actual vessels, most likely because of variation in end restraints between plate or cylindrical shapes and the effects of these boundary conditions on the crack opening displacements produced for given notch pressures. Rather large variations are also apparent for flaws of the same size in several vessels, possibly caused from (1) intermittent extended pump operations at insufficient load pressure, (2) minor pump seal and/or system leakage, and (3) uncorrected variations or regulation in the air supply pressure to the pump.

Initiation flaw growth usually is detected ultrasonically once the flaw center depth has grown about 3 mm (⅛ in.). Confirmation generally is possible by the time the growth is double this distance. AE scanning, applied first for the recent ITV-8 mock-up cylinder and vessel, also provided noise activity vs time data to influence and supplement UT growth observance. The ITV-8 pump-monitoring setup is shown in Fig. 3.

3.2 Machining Preparations

No machine tools were readily available for the early vessel tests that had the capacity to support the nearly 9.1-t (10-ton) weight of the intermediate test vessel. Accordingly, modified versions of commercially available portable tooling were used to perform required machine operations: (1) cutting the notch to the desired depth and contour, and (2) providing a precision-finished seal surface above and at right angles to the notch preparatory to flaw pumping. A masonry saw and a hand surface grinder mounted to a specially built guide bed and clamp (Figs. 4 and 5) were used to prepare the notches for early vessel tests.[3] Following the grinding, the surfaces had to be hand finished with a parallel bar and emery paper.

Preflaw machining operations on the vessel 8 prototype mock-up and the actual vessel 8 were performed in shops of the Union Carbide Corporation–Nuclear Division Y-12 Plant. The ITV-8 test called for an axially oriented outside-surface flaw to be placed in a region of high residual stress and toughness. Results of the destructive examinations conducted within an identical weld repair region of prolongation cylinder V-8, the procedure qualification unit for vessel 8, located highest residual stresses in a zone about 19 mm (¾ in.) from the repair weld's heat-affected zone (HAZ) within the submerged-arc weld metal of the cylinder's fabrication seam weld. Machine shop machinery was selected to attain the most precise index and depth control.[4,5]

An ~1.22-m-long (~4-ft) center cylinder section from previously tested and fractured intermediate test vessel V-9 served for prototype work to develop the machining-approach flaw groove preparation procedure and later to serve as a mock-up for cyclic flaw pumping. The cylinder mock-up was placed vertically onto a 127-mm (5-in.) mill table bed to generate a typical V-1 type[3] semicircular flaw notch 206 mm (8.1 in.) long by 50.8 mm (2 in.) deep at the surface of the cylinder. The contour of the notch tip was circular for the two ends joined by a straight section about 30 mm (1³⁄₁₆ in.) long at the deepest part of the notch. The straight-run portion of the notch provided clearance necessary for chip release. A number of slitting saws were used. The final saw cutter was ground to a 30° included angle with a 0.127- to 0.191-mm (0.005- to 0.0075-in.) tip radius to give the tip of the notch a sharp point. A schematic for the slot machining sequence operations is shown in Fig. 6. A flat plane was also milled onto the vessel surface perpendicular to the saw slot to establish a precision surface on which to mount a block for sealing the notch for pressurization. After the machining was completed, a silastic rubber impression of the cavity was made, from which a stainless steel matching insert was fabricated for a tight-fitting plug. The insert provided tiny side grooves to channel hydraulic oil to and from the bottom of the notch.

Flaw slot machining for the vessel followed and generally duplicated the previously described procedures. Vessel V-8, however, was placed horizontally into cradles on the bed of a large 152-mm (5-in.) Giddings and Lewis vertical boring mill for slot machining (Fig. 7). The height of the vessel prevented use of the vertical machining setup that was used for the shorter prototype cylinder. The resultant horizontal vessel positioning made chip removal from the generated slot groove difficult. Without gravity assist for dropout of chip and dust residue, the circular slitting saw cutter teeth frequently galled and dulled rapidly and at times even broke off corners. Consequently, considerable time and effort were expended in cutter maintenance. No problems were encountered in the top-of-slot surface-milling operations for a precision seal surface.

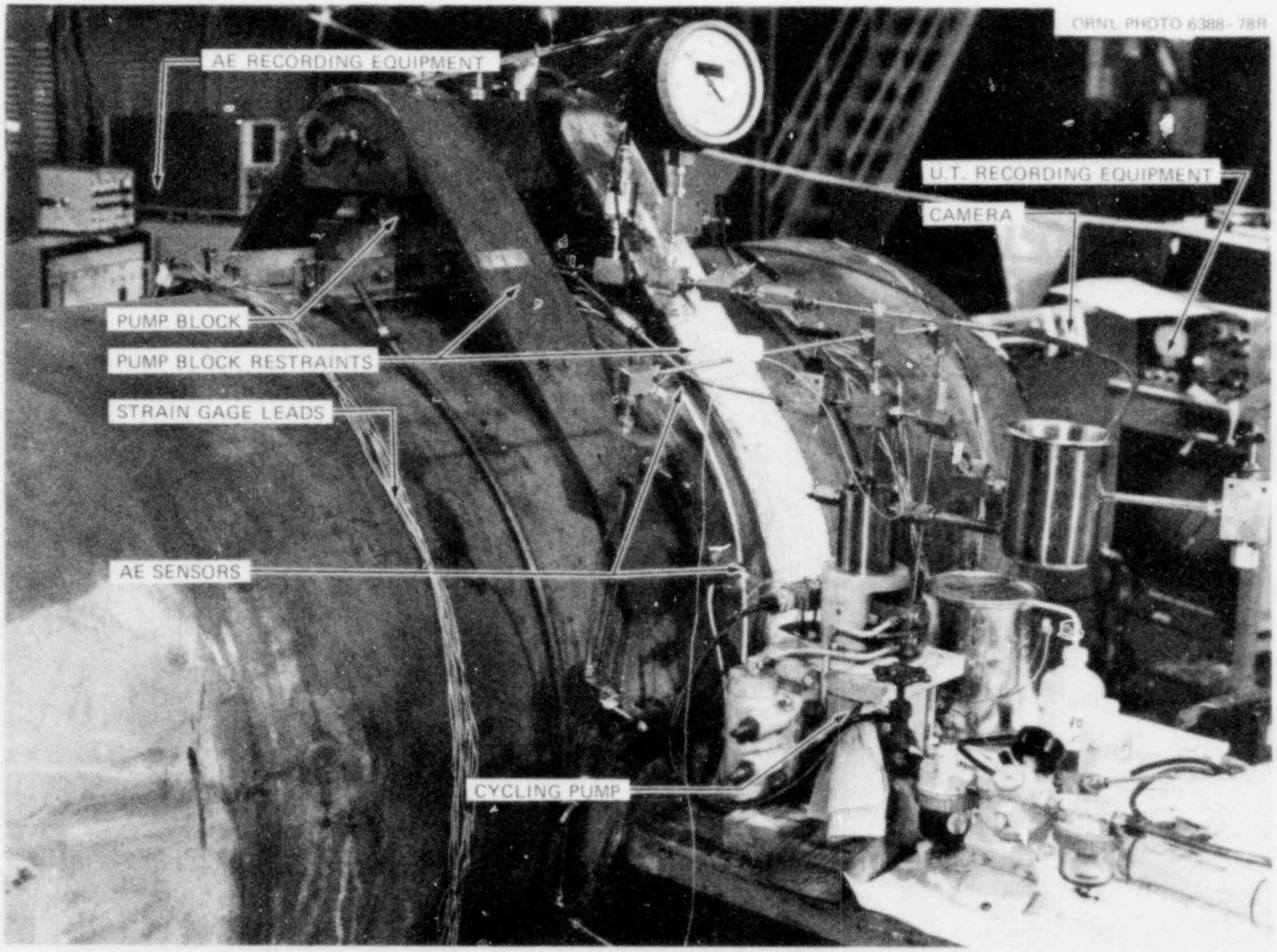

Fig. 3. Vessel V-8 during cyclic notch pressurization, showing apparatus for sealing notch and transducers for ultrasonic and acoustic emission observations.

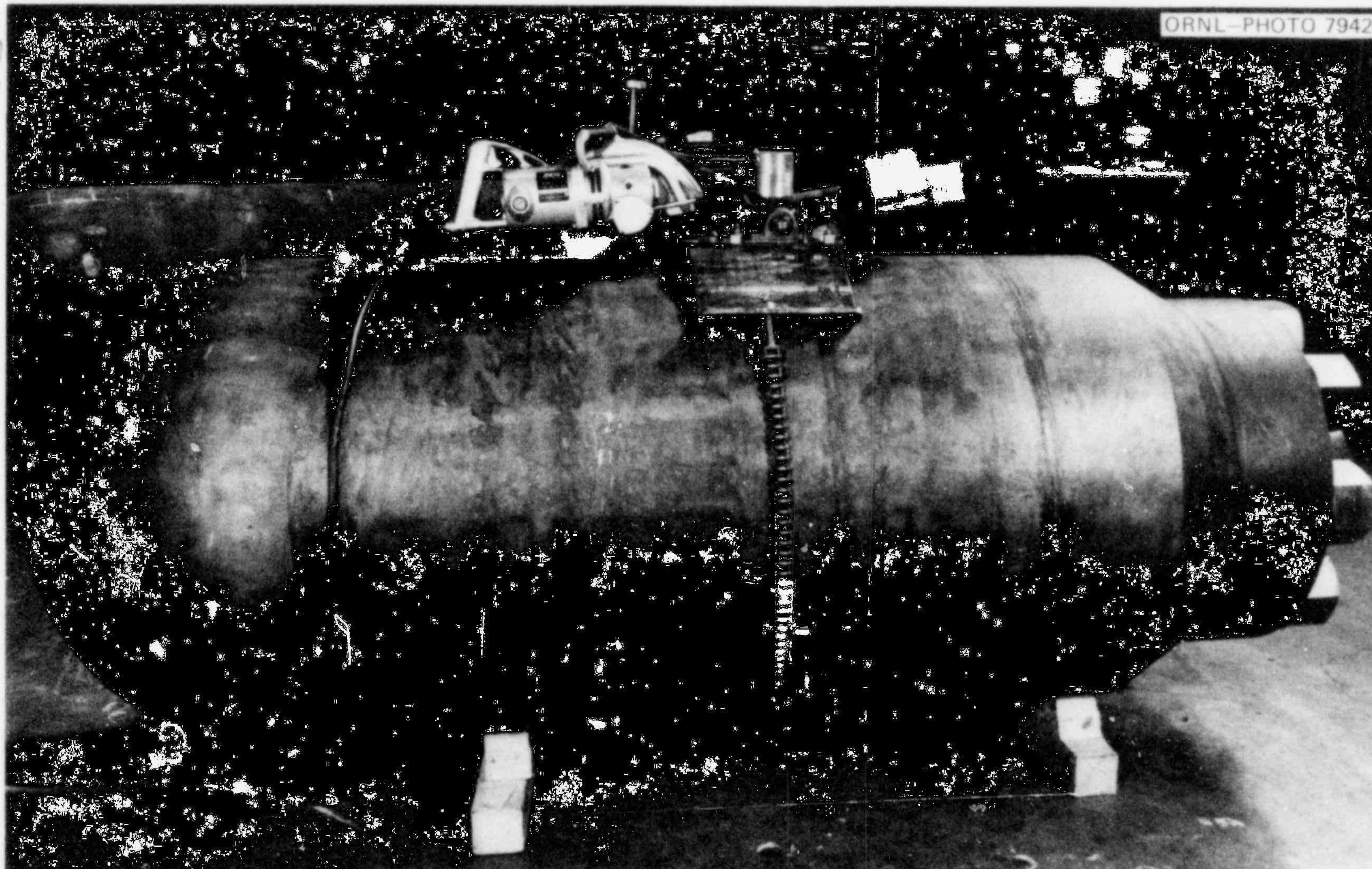

Fig. 4. Portable saw mounted on vessel in preparation for cutting notch.

ORNL–PHOTO 79424

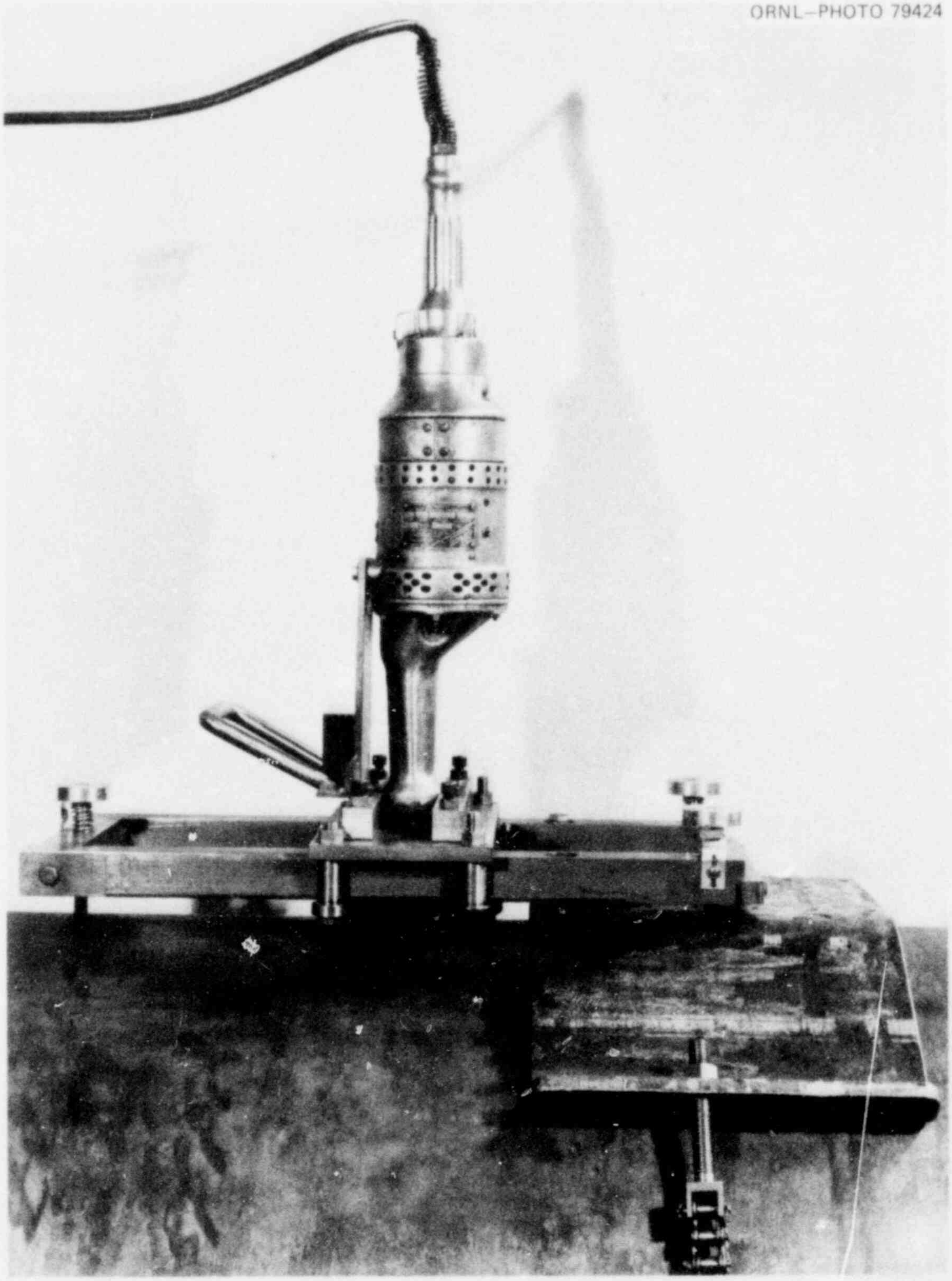

Fig. 5. Surface grinder attached to vessel in preparation for grinding a small flat area to provide a sealing surface.

ORNL-DWG 78-5997R

STEP	CUTTER	W (mm)	C (mm)	D (mm)
1	152.4-mm (6-in.) SLITTING SAW	151.46	21.42	36.50
2	203.2-mm (8-in.) SLITTING SAW	178.71	21.42	37.29
3	203.2-mm (8-in.) SLITTING SAW[a]	182.02	22.07	38.94
4	203.2-mm (8-in.) SLITTING SAW[b]	205.74	29.77	50.80

[a]MODIFIED TO 0.76/1.14-mm CORNER RADIUS
[b]MODIFIED TO 30° ANGLE, 0.13/0.19-mm TIP RADIUS

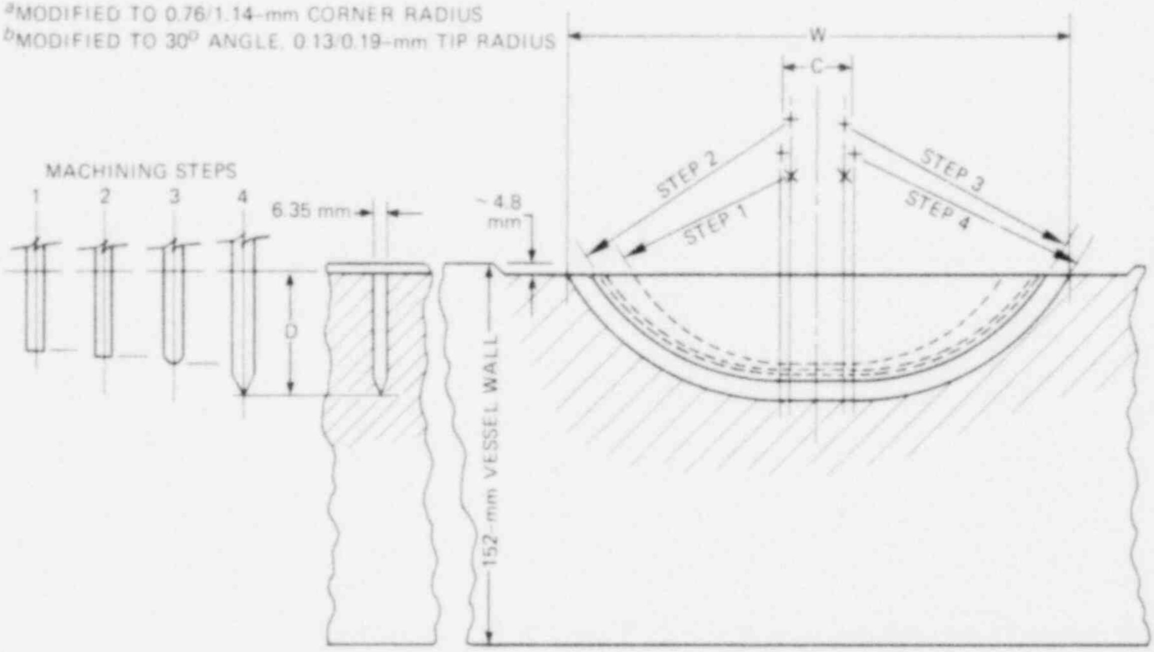

Fig. 6. Vessel V-8 slotting sequence for flaw groove machining.

3.3 Interior Nozzle Corner Flaws

The successful sharpening of a flaw on the interior wall of intermediate test vessel V-6 (ref. 6) provided basic background information required to guide the development of procedures for growing the inside nozzle corner flaws in vessels V-5 and V-9, using welded-on inside nozzle corner seal blocks. However, the task of developing a reliable procedure for growing an interior nozzle corner flaw presented considerable additional mechanical, welding, detection, and pumping problems. A number of inside nozzle corner mock-ups were built and employed to (1) develop and test sawing methods, weld boss configuration, weld penetration for adequate weld attachment, and high-pressure pump-fatiguing and UT depth-testing techniques; and (2) develop operational and test procedure standards for the work. Safety and quality assurance and quality control procedures were developed and utilized for all tasks. The following HSST Program Code 10563 ITV Crack Preparation Facilities Procedure Standards were issued:

1. Test Procedure for Safety Equipment Mobility Test,
2. Welder Qualification Test for Interior Nozzle Corner Weld-on Bosses,
3. Verification Test for Preheating Procedures,
4. Welding Procedure for Interior Nozzle Corner Weld-on Bosses,

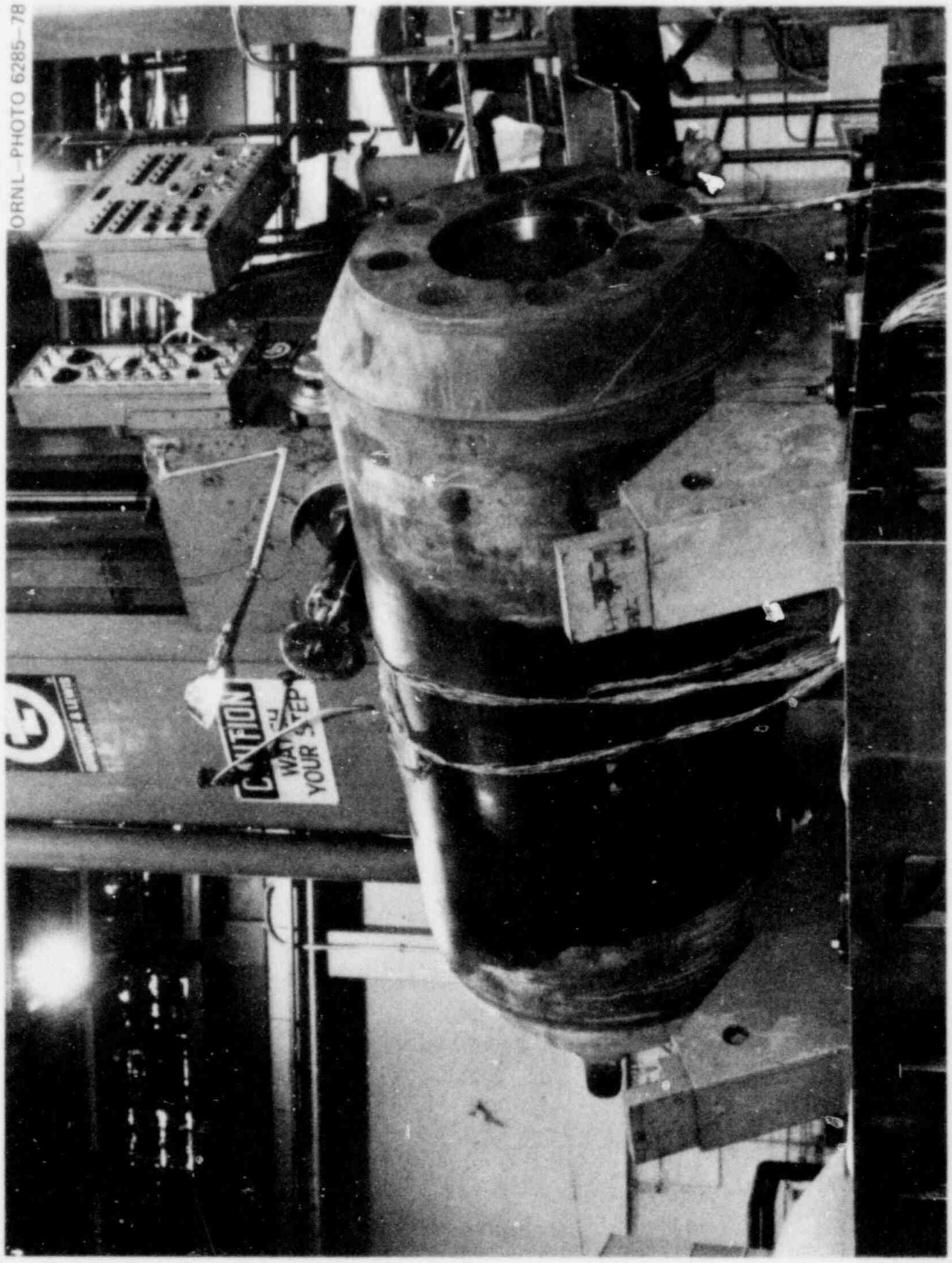

Fig. 7. Vessel V-8 slot machining.

5. Scarfing Procedure for Interior Nozzle Corner Weld-on Bosses.
6. Preparation for Mounting Transducers for Nozzle Corner Ultrasonic Monitoring.

High-pressure pump-fatiguing tasks were performed in accordance with special pump operating instructions, which are included in the appendix of this report.

Welding, notch machining, and subsequent instrumentation work inside the vessels were facilitated by the vessel support stand and elevator lift (Fig. 8). A number of safety precautions were incorporated into this facility to ensure safe entry into the vessel by a welder fully clothed with a heat-resistant, flameproof suit and attached wristlets (Fig. 9). Other special precautions included the elimination of any electrical shock hazards from the vessel, supporting structure, and protective clothing; two-way phone communications; continuous monitoring by personnel stationed specifically for that purpose; protected insulated nylon rope for wristlets that retain the welder's hands vertically upward to permit rapid assisted evacuation, if required; nonhazardous internal tank lighting; and controlled air circulation in the vessel to prevent asphyxiation.

Figure 10 shows the final notch-sawing template and weld boss pieces. The slitting fixture was contoured to match the nozzle curvature and tack welded to the nozzle corner to guide a sawblade 0.65 mm (25 mil) thick for a slot about 20 mm (0.80 in.) deep at the center. A template was then fitted to the presawed area for trimming five 0.13-mm (5-mil) stainless steel shim inserts, which were placed in the notch to reduce oil volume before the weld boss cover was aligned. Tabs placed beforehand on the shims served to align the weld boss properly over the slot, while interior fixturing supported the boss for weld tacking and root-pass operations.

American Society for Testing and Materials (ASTM) A533, Grade B, Class 1 plate was selected for the weld boss material to match the vessel steel and the vessel manufacturer's weld electrode selection (E-8018) used for welding the nozzle forgings to the vessels. Care was taken to retain planar coordinates for the weld block orientation to match that of the vessel wall.

Development trials indicated the need for considerable weld penetration for the weld-boss-to-nozzle attachment to ensure fatigue crack growth in the plane of and beyond the sawed slot rather than through the outer edges of the weld joint. Figure 11 represents the final cross section of the flaws grown in the nozzle corners of vessels V-5 and V-9. Flaws in both vessels appeared to be generally similar, of nonuniform or irregular depth, and with nearly identical amounts of visible fatigue crack growth on the inside surfaces of the nozzle and vessel. The 11.7-mm (0.46-in.) fatigue crack growth dimension shown in Fig. 11 is based on posttest measurements; the other dimensions shown in the figure are pretest estimates. For a visible external fatigue crack of ~16.5 mm (~0.65 in.) on the horizontal and vertical surfaces of the inside nozzle, or ~11.7 mm (~0.46 in.) in the plane of the sawed nozzle slot, boss blocks as shown in Fig. 12 beveled for welding to provide double those distances for weld deposit fill proved adequate. In earlier trials with separate pump oil inlet and outlet connectors, fabricated from bar-shaped stock and with single-unit dual-connector weld boss units of smaller size, cracks developed, causing oil to leak through the weld metal edges before the desired "pumped-flaw" depth was achieved.

Four weep holes were precision machined into each weld boss block (Fig. 13) to establish a leak passage for the pumped oil when the fatigue crack had grown to a depth of ~12.7 mm (~½ in.) beyond the bottom of the presawed notch in the vicinity of the notch midpoint. The weld boss holes served as fixtures for aligning and guiding the drilling of the weep hole passage extensions into the nozzle. For each vessel, two holes were drilled until the hole intercept depth was reached. Four holes were available in the weld boss (Fig. 13) in case drills should break, but these holes provided only questionable confirmation of fatigued flaw depth. Oil traces were noted, in the case of vessel V-5, at an actual fatigue

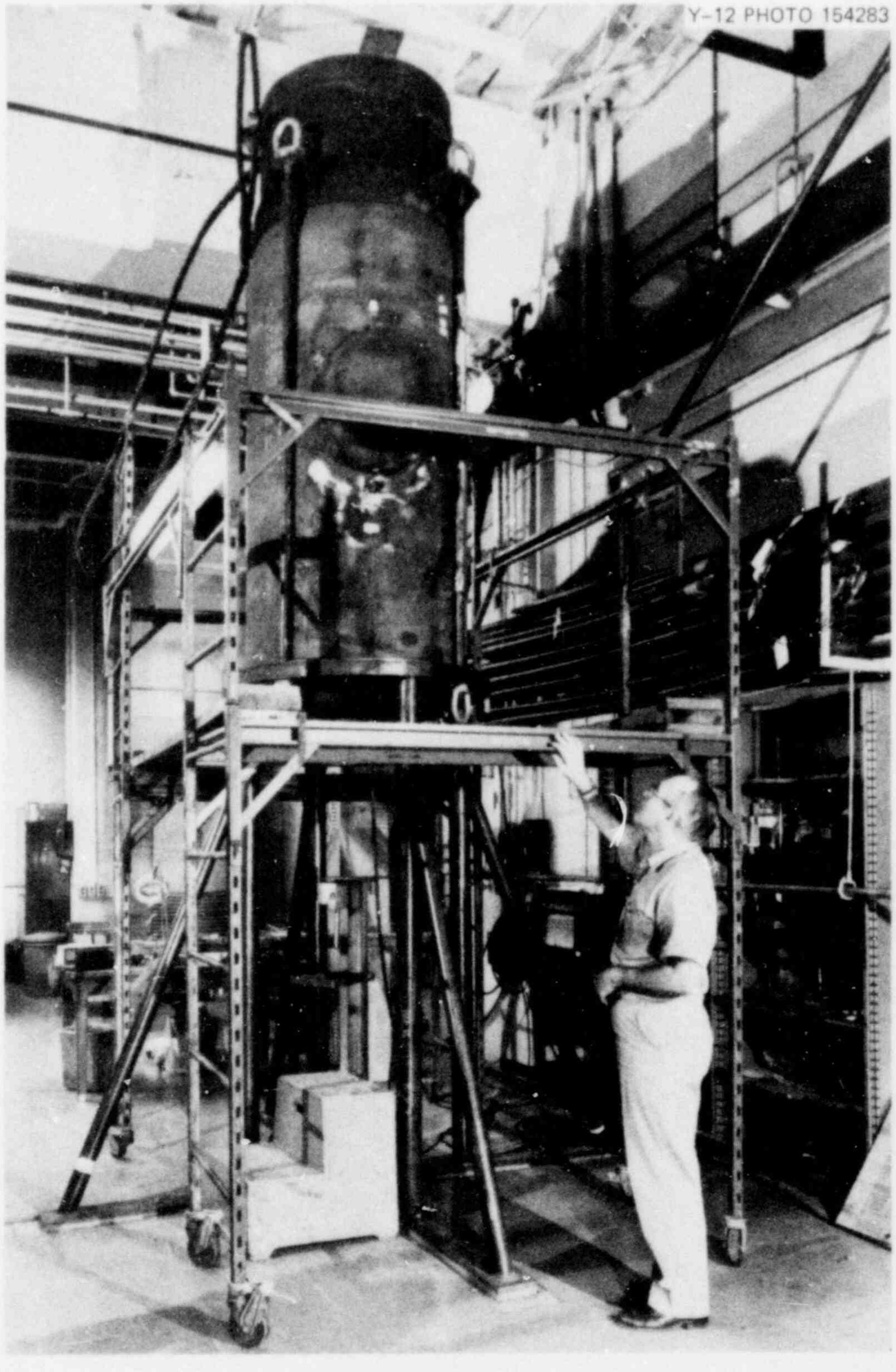

Fig. 8. Vessel support stand and elevator lift.

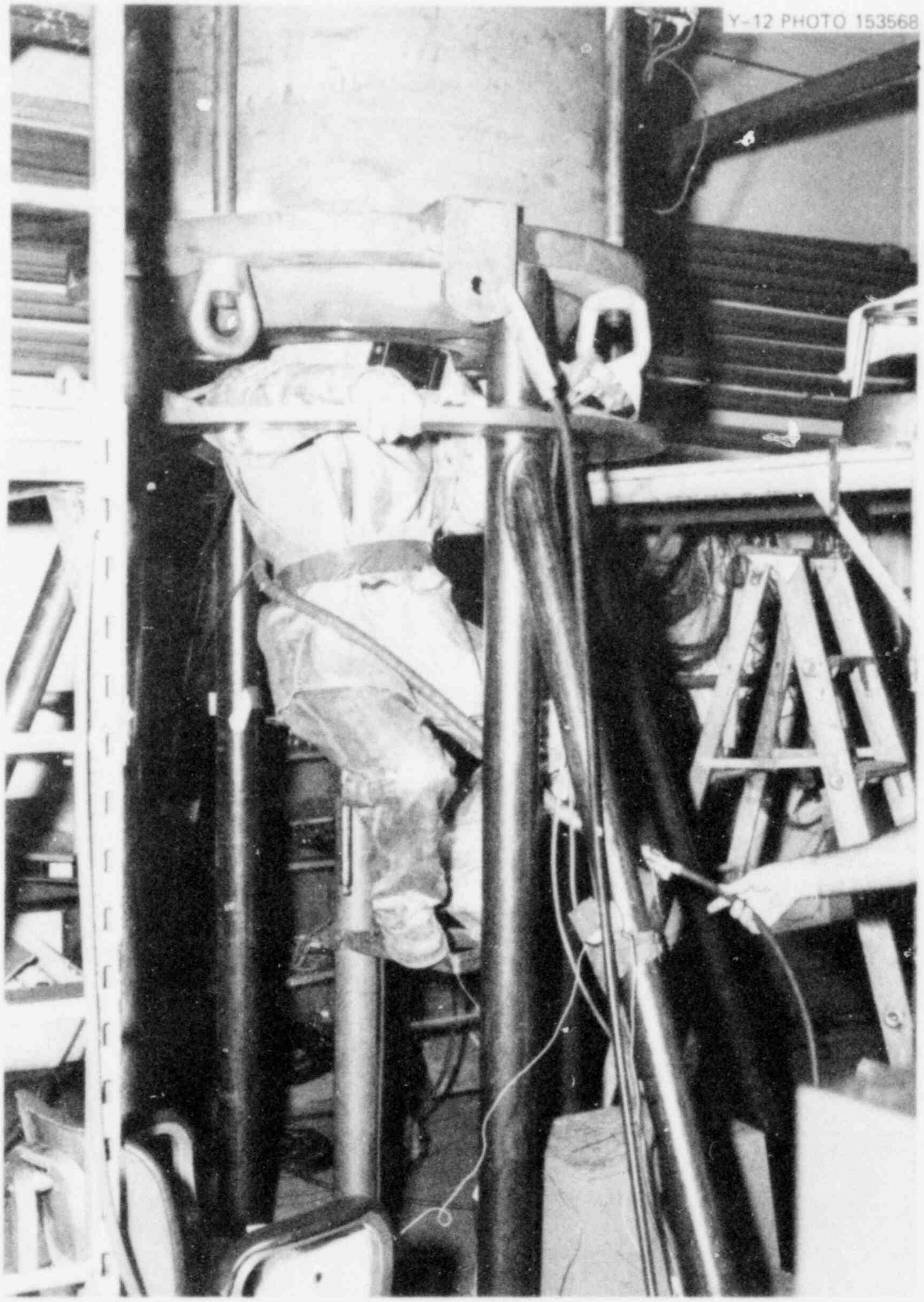

Fig. 9. Welder entering vessel V-5.

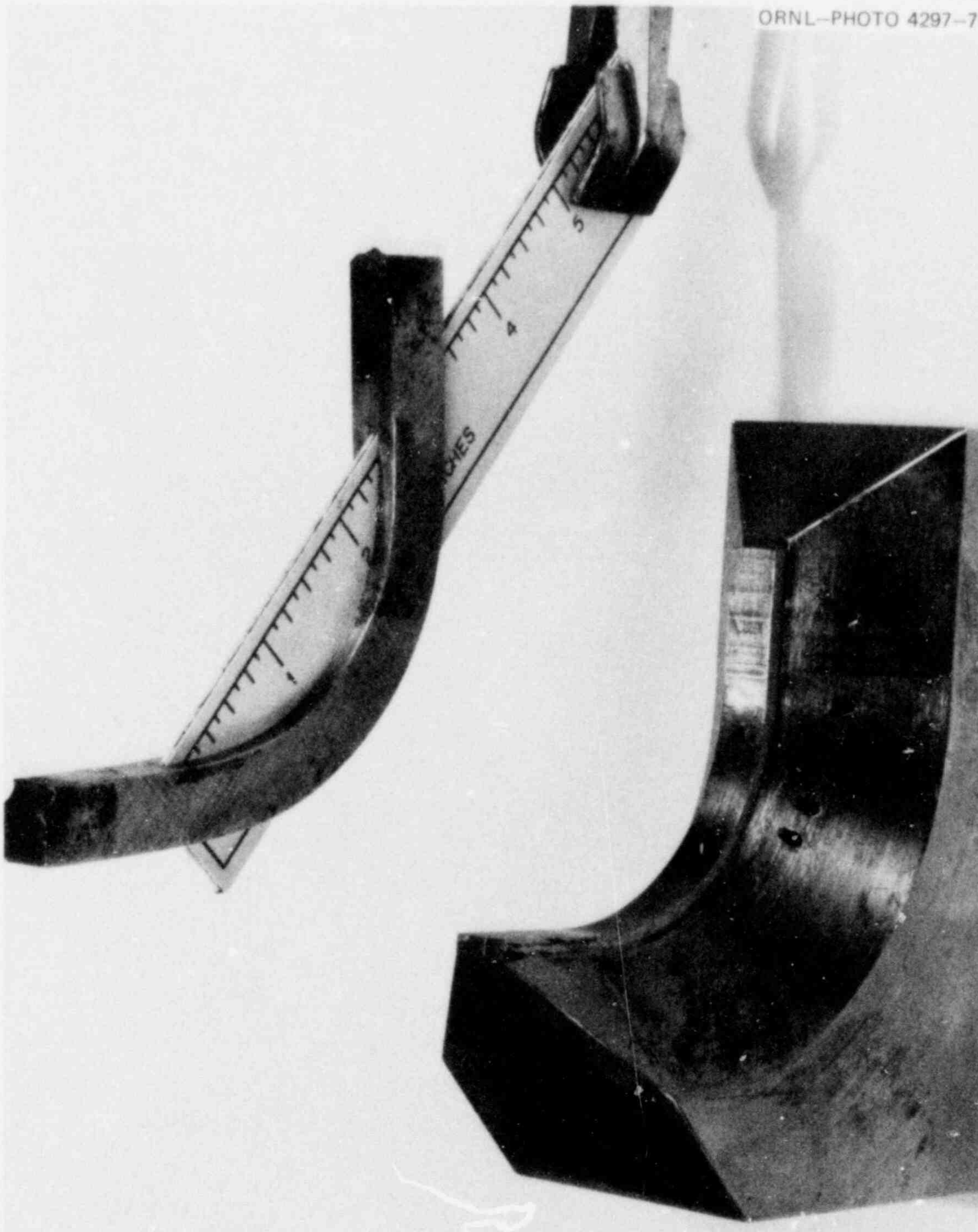

Fig. 10. Weld boss and sawing template fixtures used in preparing and sharpening flaws in vessels V-5 and V-9.

ORNL-DWG 74-6929R2

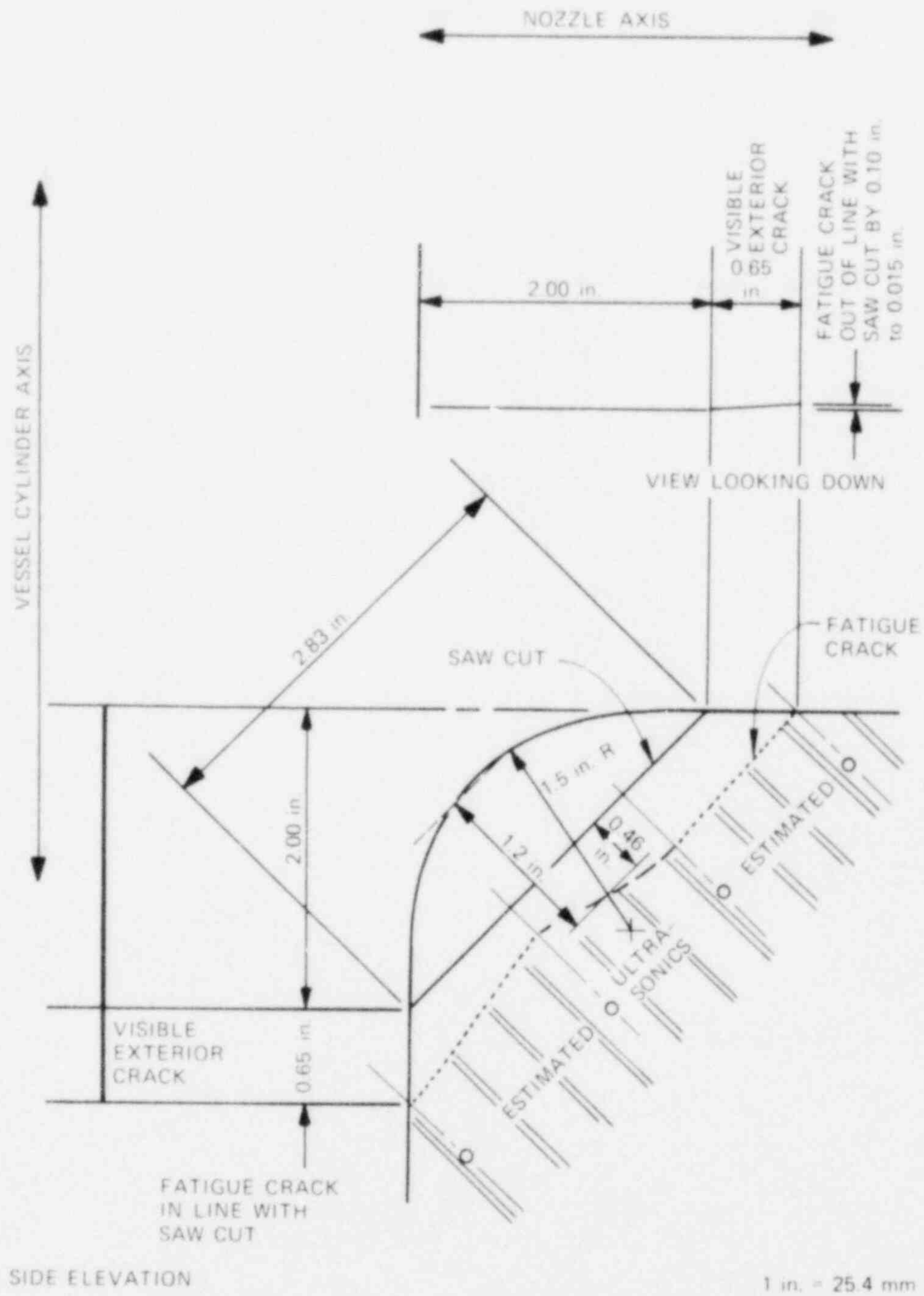

Fig. 11. Cross section of inside nozzle corners, showing flaws in vessels V-5 and V-9.

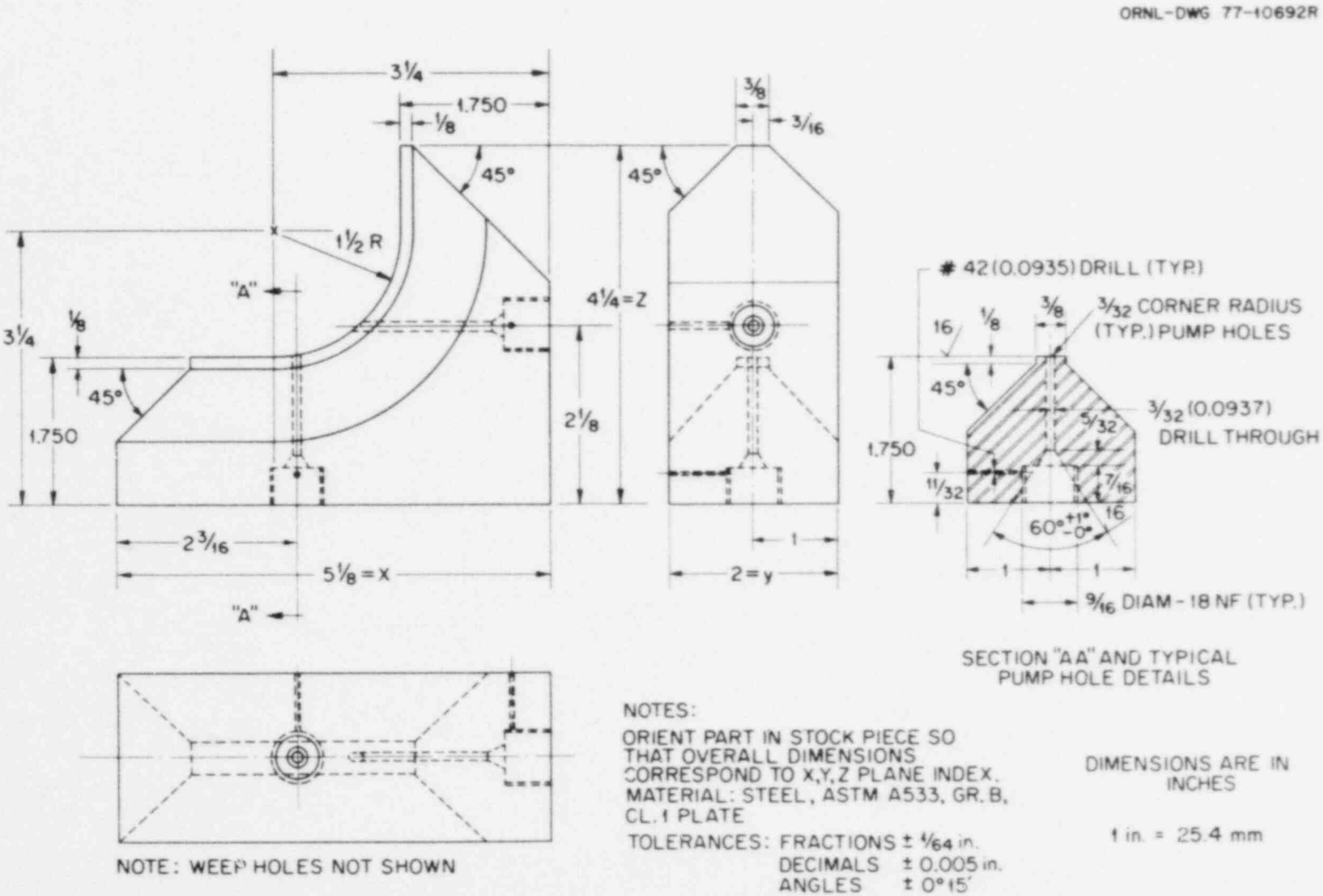

Fig. 12. Nozzle corner weld boss design for vessels V-5 and V-9.

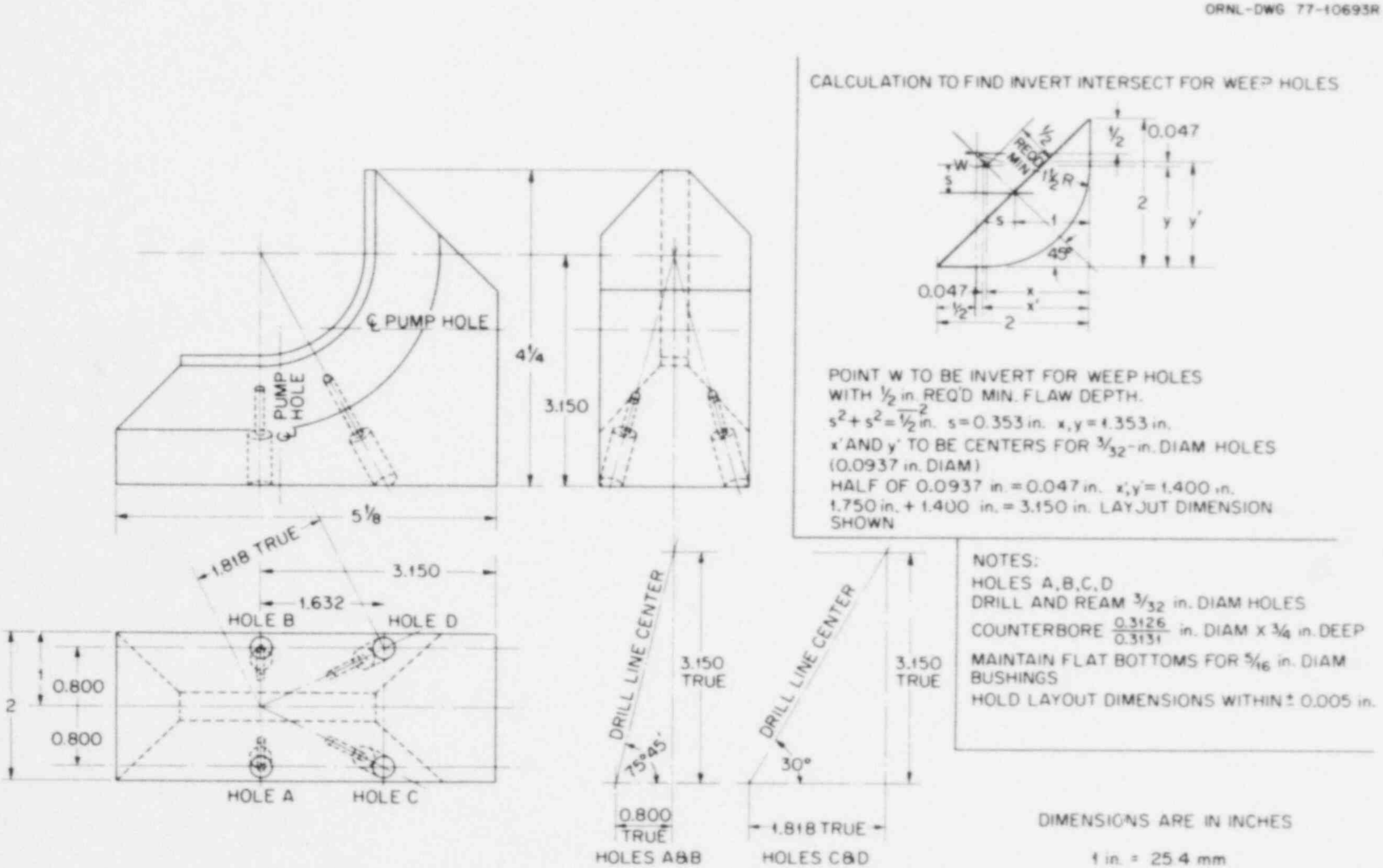

Fig. 13. Weep hole design used for weld bosses in vessels V-5 and V-9.

crack depth that later was observed to be slightly less than the originally intended 12.7 mm (0.5 in.) at the notch midpoint. Oil leaked from one of the monitor holes in vessel V-9 shortly after pumping was started, and the monitor passage had to be plug welded to seal off a crack that had grown from near the invert of the weld boss oil inlet connection into the weep hole passage. The entire crack was found to have formed within the weld boss block, external to the boss-to-nozzle weld. Therefore, depth estimates of nozzle corner flaws had to be based on UT measurements made from the outside surface of the nozzle, directly opposite the crack.

The cyclic loading applied to the notches for both vessels V-5 and V-9 was about 172 MPa (25,000 psi) oil pressure for ~225,000 cycles, each cycle requiring four pump strokes. Under ideal operating conditions, the system can average about 50 to 52 cycles per hour.

Welder qualification certifications were held on mock-ups to prepare the welder for working in the special clothing within confined spaces and to demonstrate that all required welding operations could be performed.

Local preheating of the weld boss and the adjacent nozzle and vessel walls controlled boss and wall temperatures for the boss weld-on process to within a range of 177 to 288° C (350 to 550° F). Vessel surface temperatures were also monitored and were controlled not to exceed 316° C (600° F). Electrical Calrod heating, occasionally supplemented by manual torch flame heating to the vessel's exterior surface, was used, along with an insulation blanket liner within the vessel. The preheat was controlled and monitored via thermocouples. Postwelding temperature was maintained between 232 and 288° C (450 and 550° F) for 2 h and gradually reduced thereafter. E-8018 filler rod was used for the root pass, which was made by the gas-tungsten arc process with a specially shaped torch tip to reach the entire periphery of the pass. The vessels were allowed to cool down for liquid dye-penetrant testing of the root passes before we proceeded with renewed preheat and additional gas-tungsten arc passes and finally manual metal arc passes using E-8018 weld wire procured specifically for this purpose. Interpass temperature was controlled to 288° C (550° F). The completed welds again were checked with liquid dye-penetrant. Figure 14 shows the completed vessel V-5 weld boss and cyclic pressure connection, which was photographed with the aid of a mirror in the vessel.

Flame-cutting techniques were used for the removal of the weld bosses from the vessel interiors. Oxyacetylene torch gouging followed "crack-sharpening" operations, with the vessels placed horizontally and preheated locally by a torch to about 177° C (350° F). The flame-cut surfaces were kept a minimum of 3.2 mm (⅛ in.) from the inside surfaces of the vessel. The remainder of the protruding metal then was removed by hand grinding to 6.35×10^{-3}-mm (250-μin.) finishes so that the finished surfaces would conform to within 1.6 mm ($^1/_{16}$ in.) of the true position of the inside surface.

Shallow weld pads were joined to the circular external nozzle fillet contour of vessels V-5 and V-9 to provide a plane perpendicular to the plane of the flaw and parallel to the root of the saw cut. Each pad served as a base for a sleeve that positioned and housed a UT transducer. The transducer crystals transmitted information on the depth of the flaw center during flaw pump-cycling operations and served to terminate pumping upon reaching an ~30.5-mm (~1.2-in.) center flaw depth, or about 10.2-mm (0.4-in.) growth in depth beyond the saw cut. Actual posttest measurements at the exact flaw center indicated slightly lesser depths [about 7.6 mm (0.3 in.)] but showed an irregular fatigue flaw depth contour to establish 30.5 mm (1.2 in.) as the average center depth.

3.4 Monitoring

Several UT techniques have been used to measure crack depth with varying degrees of success. On the 15.24-cm-thick (6-in.) tensile test specimen, a longitudinal wave was projected along the length of

ORNL-PHOTO 4000-74

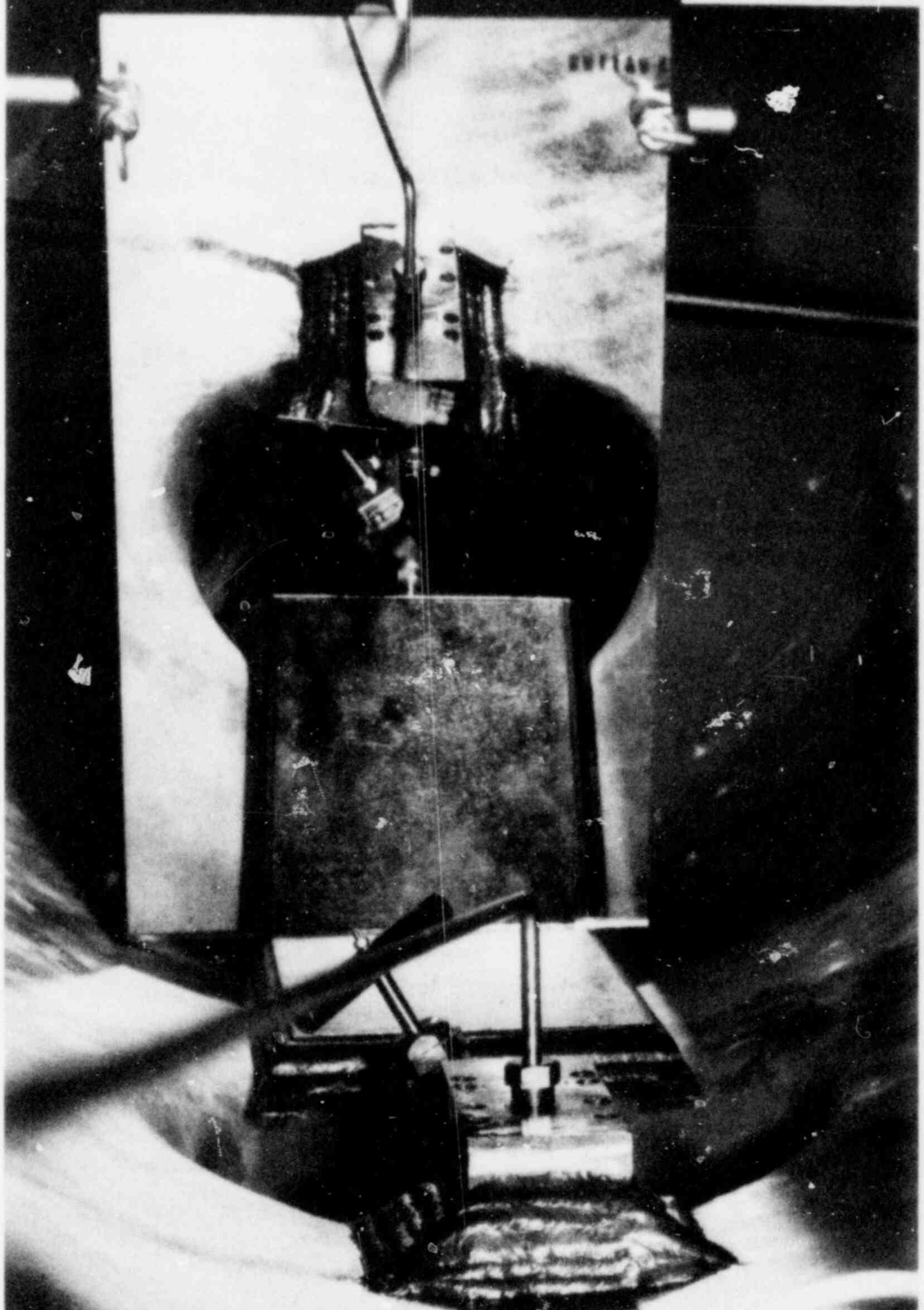

Fig. 14. Mirror view of weld boss with pumping attachment for sharpening flaw on vessel V-5.

the specimen, and the crack tip was followed by correlating through-transmission signals and echo signals with transducer movement. The method provided an accuracy of about ±2 mm.

With the HSST test vessels a similar technique was tried, except a 60° shear wave was projected along a chord of the vessel wall. The transducers were mounted on OD surface tracks to obtain scan reproducibility. Again, the crack depth was inferred by correlating through-transmission signals with transducer location as the crack depth increased. Initial results on prolongation samples were good, as were the results on the first two vessels monitored. The data on which depth determination was based, however, became too scattered with subsequent vessels to give good assurance of reliability in determining the crack depth.

Concurrently with the shear wave monitoring, other methods were sought for more accurate measurements. These efforts were directed toward detecting the UT energy radiating from the crack tip when excited with a strong sound pulse. This method was partially successful; however, a phenomenon was observed that led to a more accurate method.

At the amplified gain levels being used, considerable noise (grass) was present along the entire baseline. These noise signals result from an interference pattern generated by return energy from within the metallurgical structure of the vessel wall. The noise pattern was stationary along the entire baseline except for a short length where the crack was growing. The noise pattern would change rapidly with each notch pressurization cycle. Further observation revealed that the length of the moving noise region increased with cycling time. A few samples confirmed that the span of the moving noise region was directly related to the crack depth.

An epoxy-faced transducer of 5 MHz has yielded the best results. The three criteria for the method are short wave length for accuracy, metal noise at a gain low enough to prevent electronic noise, and pressure cycling of the crack. A transducer mounting surface parallel to the crack face also improves accuracy of measurement, and pads built up on the surface have been used to achieve this when necessary. This technique has enabled crack depth to be measured ultrasonically to an accuracy of ±1.5 mm ($^1/_{16}$ in.) with good reliability.

4. METALLURGICAL FLAWING METHOD

Our metallurgical technique to generate and produce sharp cracks in ASTM A533, Grade B and ASTM A508, Class 2 steels involves autogenous EB welding followed by electrochemical hydrogen charging.

4.1 Electrochemical Process

The production of cracks in low-alloy, high-strength steels is premised on the role of hydrogen in the formation of cracks in ferritic materials. It is well established that hydrogen is responsible for underbead cracking in the HAZ of ferritic weldments. Further, such cracking is associated with stresses and microstructure. In 1970, D. A. Canonico and J. D. Hudson devised a technique to produce martensite with suitable microstructure for cracking within a zone of high residual stress and, thereafter, utilize a pool of electrolyte and a battery charger for "pumping" hydrogen to the martensite.[7] Their experimentation was based on the fact that martensite can be produced in these steels by rapid cooling from the austenitic temperature range. Use of an EB welder to place an autogenous weld on the surface of the steel assured that the heat effectively concentrated in a small region, resulting in high residual stresses of yield point magnitude. Highest stresses form along a very narrow band on the weld's chill zone located along the weld bead's centerline. The final requirement for cracking, the presence of hydrogen, can be accomplished by charging the steel, wired as the cathode at the lower potential, in a pool of electrolyte. A lead bar positioned above the weld bead's top surface serves as the anode. Figure 15 illustrates the hydrogen-charging process for a specimen submerged in a typical 10% H_2SO_4 electrolyte solution. A typical charging operation for a thermal shock prolongation is shown in Fig. 16. The specimen containing the weld is masked with a room-temperature vulcanizing material so that only the weld contacts the electrolyte. A current density of about 7.8×10^{-4} A/mm^2 (½ A/in.^{2}) of unmasked area is generally sufficient to cause a crack within 25 to 100 h. UT monitoring is displayed on the Immerscope, which is shown below the Clevite Acoustical Emission Event Recorder in Fig. 16. The UT crystals are mounted on the cylinder's outside surface in the plane of the flaw. The UT monitor indicates a shift in wave pattern display as the crack forms and propagates. The AE chart records the frequency of noise signals associated with the release of hydrogen from the weld during charging.

Cracks formed by hydrogen charging of electron- or laser-beam welds are quite similar to those produced by mechanical flawing techniques. The cracks appear to form from the root or bottom of the weld, where induced stress concentrations are the greatest, and propagate generally through the center of the weld bead's chill line to terminate along the midplane of the bead's top surface as shown in Fig. 17, a typical transverse section of a "cracked weld." The similar typical longitudinal section view is shown in Fig. 18. Section preparations for the Fig. 18 illustration entailed sawing the charge-flawed specimen into a narrow (~22-mm-wide), shallow (~25-mm-deep, equivalent to crack depth plus ~8 mm of restraint stock) bar shape for placement into an oven at ~260°C for heat tinting. The heated bar was then dropped into a bucket filled with liquid nitrogen at −196°C. Wedges were subsequently used to sever the chilled bar into halves.

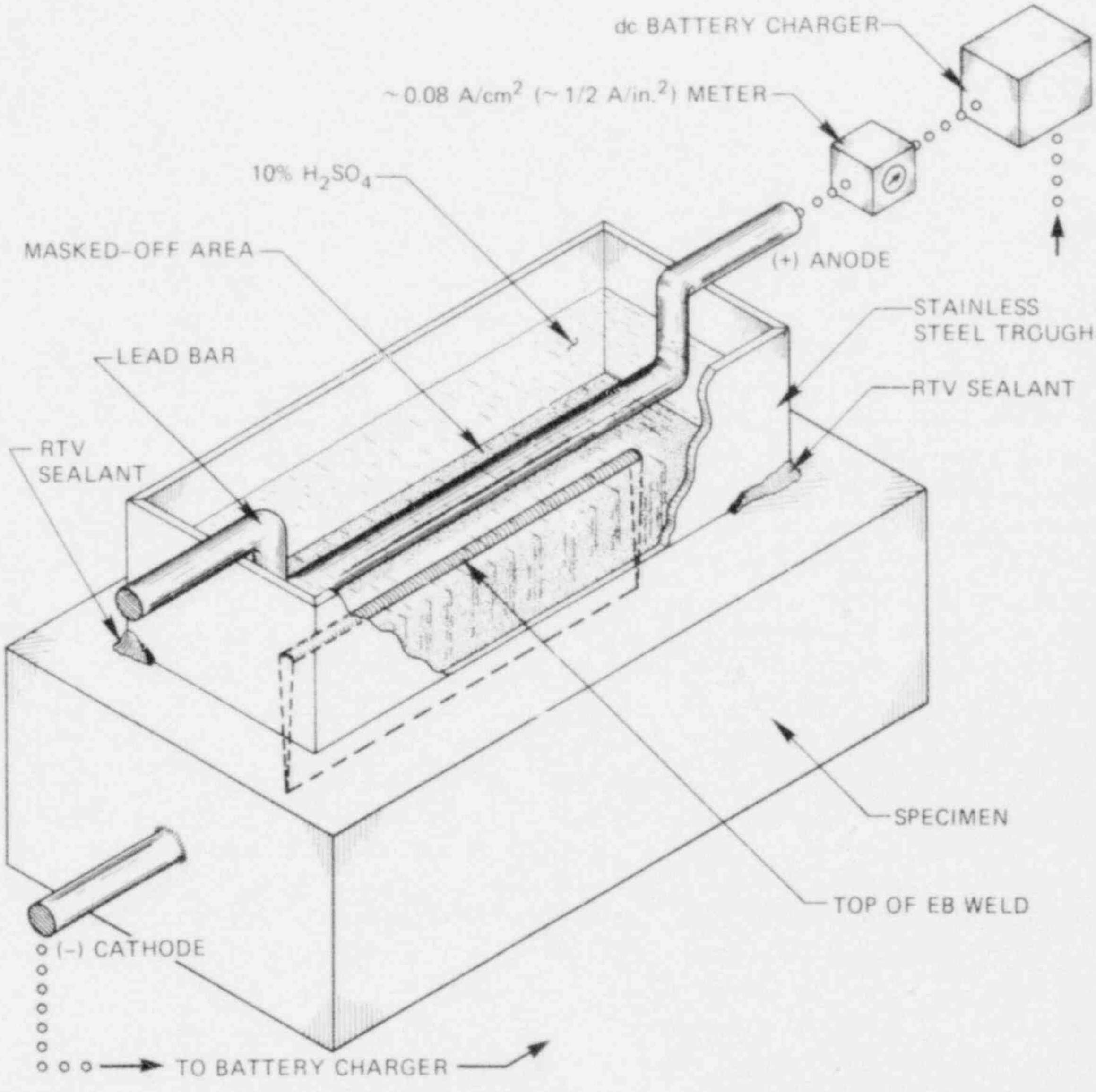

Fig. 15. Schematic of hydrogen-charging setup.

4.2 Electron-Beam Process

The following résumé functionally describing EB gun construction, theory, and nomenclature is included to review briefly how an EB gun operates. The principal parts of the EB gun (Fig. 19) are:

1. a heated filament, the source of and the emitting surface for electrons, referred to as the cathode;
2. an electrode for the formation of the beam, called the control electrode;
3. an accelerating electrode which is brought to high voltage to control the velocity of electrons in the beam, identified as the anode;
4. a magnetic coil for shaping and concentrating the beam, called the focus coil.

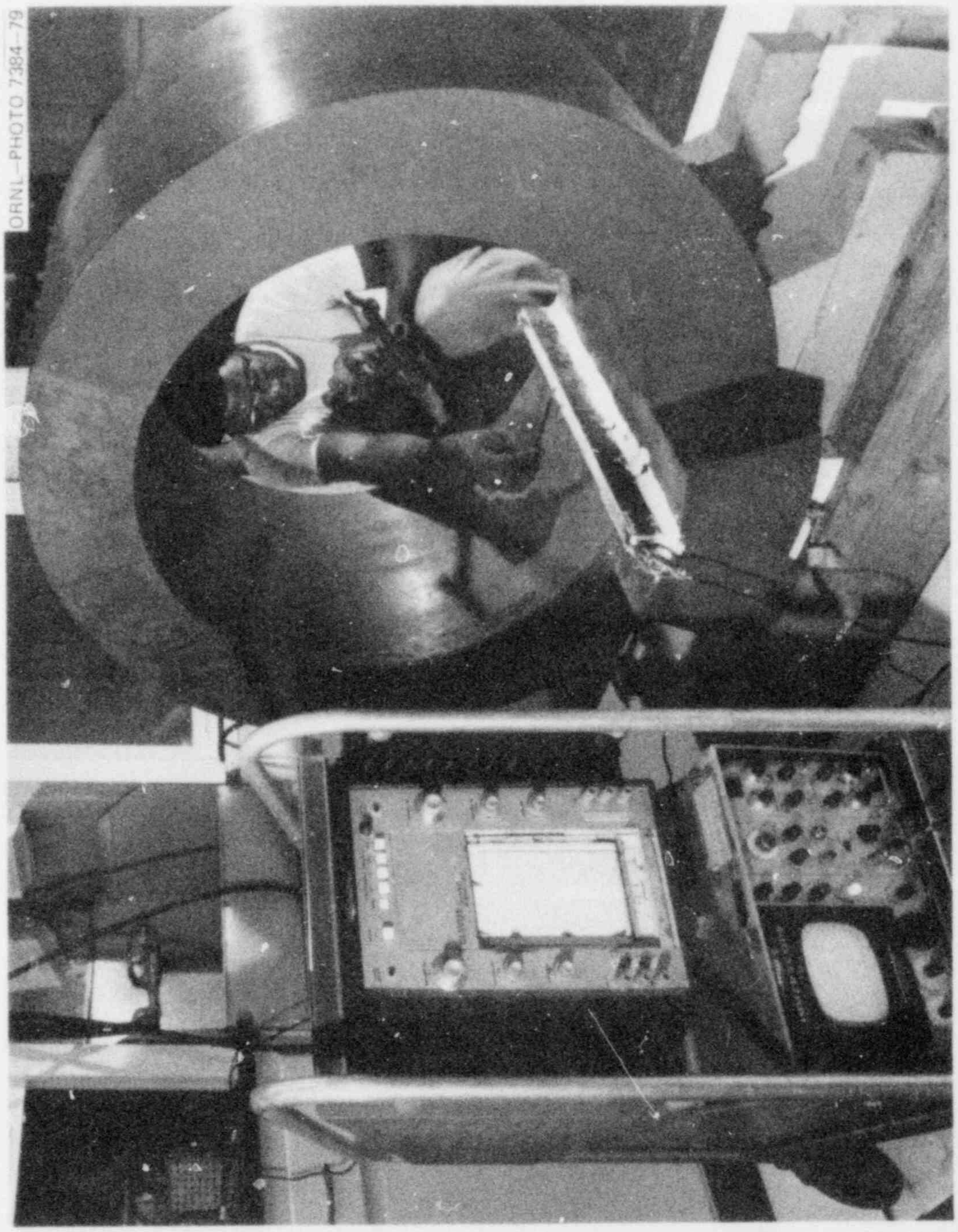

Fig. 16. Hydrogen-charging thermal shock prolongation TSP-1.

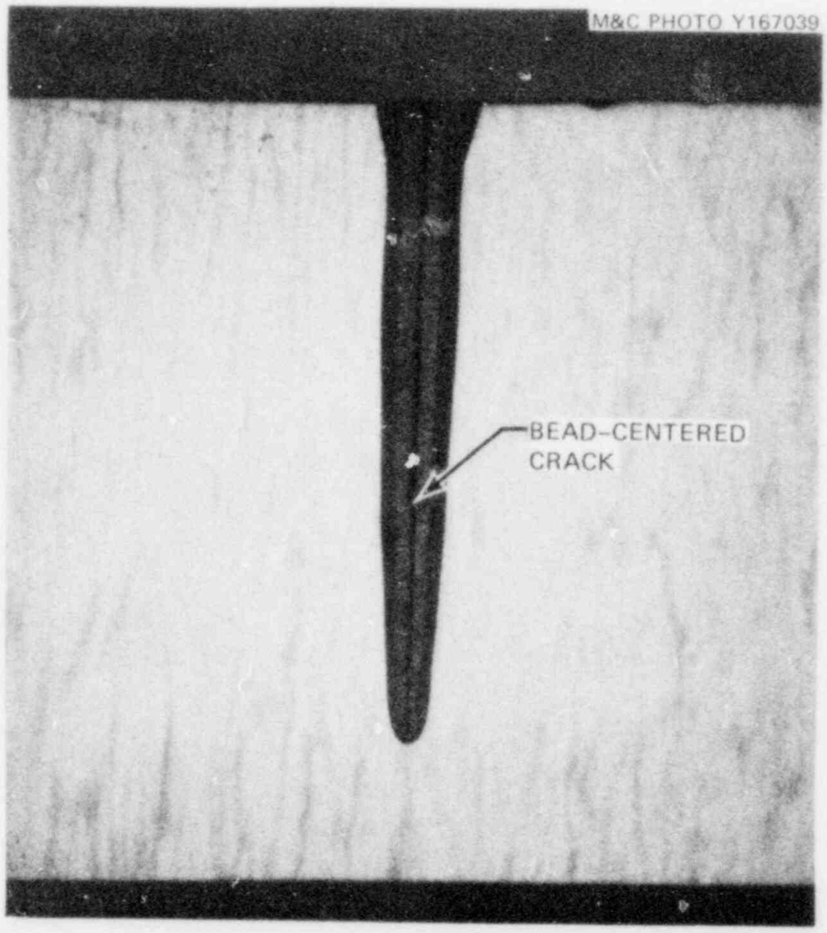

Fig. 17. Transverse cross section of an EB flawing weld cracked by hydrogen charging.

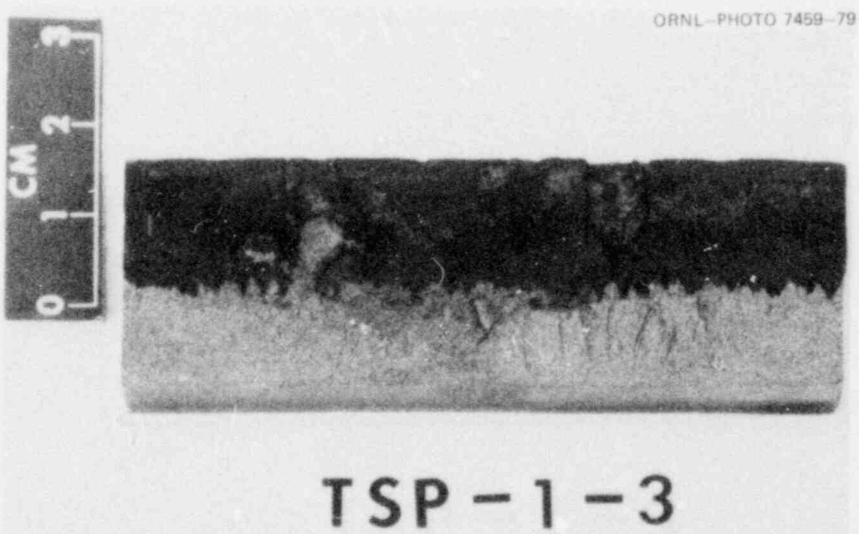

Fig. 18. Longitudinal section of an EB flawing weld cracked by hydrogen charging.

ORNL-DWG 80-4262 ETD

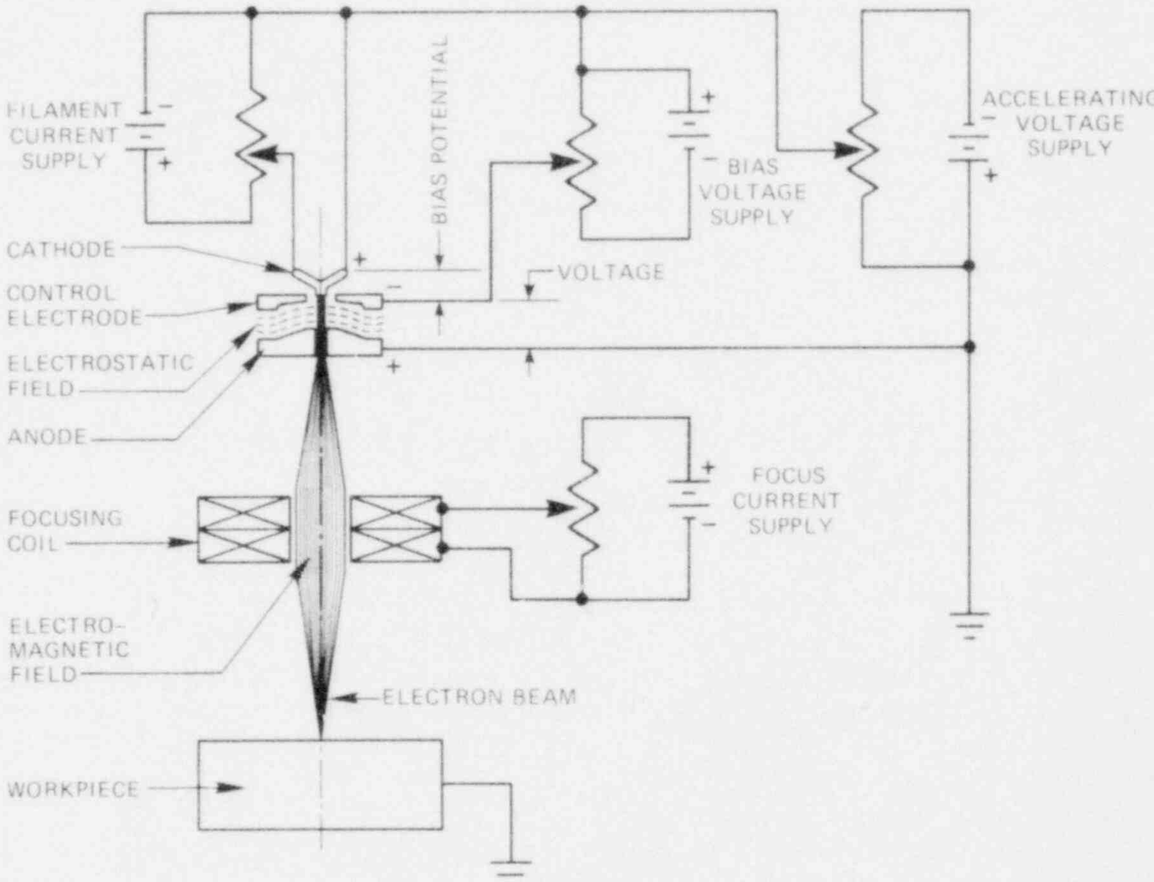

Fig. 19. Schematic of EB gun system.

By varying the bias on the control electrode between the cathode filament and the anode, it is possible to vary beam power and modify the shape of the electron trajectories in the gun. The anode in electronic tubes collects electrons. Anode construction in a welding gun, however, includes a small centered passage through which the beam passes on its way to strike the workpiece target. An electric field predominates within this upper part of the gun, or between the cathode and the anode. This region is referred to as the gun's electrostatic part. Here space charges, or effects of mutual repulsion of the electrons, cause beam divergence. The magnetic focusing coil, some distance below the anode, is then used to reconcentrate the electrons and shape the electron trajectory for convergence with the workpiece. The region located between the anode and the target, where the magnetic field dominates, is referred to as the gun's electromagnetic part.

Because EB welding is a welding process requiring minimum heat input, it normally is used to preserve special material characteristics in the parent metal. The outstanding feature of the process in which the workpiece is bombarded with a dense stream of high-velocity electrons is its ability to make very narrow, deep, single-pass welds. The EB produces intense local heating that figuratively vaporizes a hole deep into the metal. The walls of such a hole are molten, and as the beam is moved along the joint, more metal on the advancing side of the hole is melted. The melted material flows around the bore of the beam and solidifies along the rear, thus making the weld. Heat input in EB welding is controlled by four basic variables: (1) the number of electrons per second (beam current) impinging on the workpiece, (2) the electron speed at the moment of impact (accelerating potential), (3) the diameter of the beam slightly above or within the workpiece (beam focus or beam spot size), and (4) the traverse speed.

Precise cathode filament placement within the weld gun, maintenance of filament preheat current just below the filament's peak setting, and constant cathode-to-anode spacing must be predetermined, be preset, and stay fixed for developing EB weld parameters. The maintenance of a nearly constant distance between gun and workpieces, however, is most critical for autogenous EB welding to retain the proper preset focus and thereby concentrate weld heat to result in forming residual stresses of yield point magnitude, all contained within a very narrow band with a uniform pear- or spike-shaped cross-sectional bead profile. Such beads, placed at fast weld speed into work specimens large enough to provide adequate heat sinks, will chill rapidly enough to form high residual stresses and a martensitic center bead structure, which can then be made to crack electrochemically by hydrogen charging.

4.3 Electron-Beam Weld R&D Findings

Characteristically, EB welds are low heat input per unit length welds with very large depth-to-width ratios and very narrow HAZs. In EB welding, a well-defined stream of high-energy electrons is used to bombard the work material to produce a fusion joint. The energy densities developed in EB welding are considerably greater than those of the more conventional welding processes; hence EB welding tends to cause some undesirable features such as "spikes," "cold shuts" (incomplete fusion), and, at times, base porosity.

There are two modes for EB welding: the low- and high-power modes. In the low-power mode for welding to penetrations in steels to ~5-mm (~$^3/_{16}$-in.) depths, electrons give up their heat at the surface of the metal and the joint is then welded by conduction just as in gas welding, with transverse cross sections similar to sections through tungsten arc or oxyacetylene welds. In the high-power mode for deeper penetrations, the electron stream is highly concentrated to "drill" a hole by a complex thermal process, including vaporization of the metal. As the beam moves along the work, molten metal flows in behind and fills the cavity. The cavity also fills with metal vapors and gases liberated from the base metal. There is a constantly changing pressure in the hole, causing frequent eruptions of molten metal observable atop the bead as "berries" or weld spatter. Researchers[8] claim to have observed the EB oscillating up and down along the vertical axis of the cavity that the beam generates during the welding operation. Beam oscillation occurs in the weld cavity as a result of these dynamic fluid forces of the molten metal combined with vaporized metal atoms that are constantly in an unbalanced state. Irregular cavity closures are formed by the molten metal flow, which intersects the weld beam at various heights along the vertical axis of the weld cavity to yield a constantly changing weld beam focal distance. These changes in effective weld-gun-to-work distance show up as spiking characterized by an uneven, ragged root appearance. A spike may also be defined as a sudden increase in weld penetration beyond the average weld penetration depth line. Spiking is normally associated directly with voids or incomplete fusion pockets resembling porosity inclusions located slightly above the average weld penetration contour. Figure 20 exemplifies a spiked longitudinal cross section of a deep partial-penetration EB weld in carbon steel material. Spiking phenomena are eliminated in full-penetration EB welding where gases and vapors are vented through the bottom of the weld, with conditions in the "forming" weld cavity region reasonably constant.

ORNL–PHOTO 6926–79

Fig. 20. Longitudinal crack-line section of a deep partial-penetration EB weld in carbon steel, showing typical spiked profile.

Experimental procedures[9] have been developed with X-ray pinhole cameras to record events occurring as an EB weld cavity is formed. Direct correlations were made between the location of the exposure on the film and the location of the source of X radiation to reveal the location in the weld cavity where electrons from the beam collide with metallic atoms because X radiation is emitted from such collisions. The experimenters observed the EB to impinge on the liquid surface of the base of the weld cavity, which was the penetration recorded by the film. By later cracking open the partial-penetration butt joint and measuring weld penetration, they noted that they had actually measured the height of the cavity, plus the thickness of the metal layer at the cavity base, plus the thickness of a region that was later melted by thermal conduction as the beam moved on. The thickness of this "liquid" layer at the cavity base was observed to be about 2 to 4% of the total penetration depth. In X-radiation technique development, the investigators also noted "closure explosions" by vaporization to cyclically clear the cavity of liquid and allow the EB to impinge on the cavity base to form a spike. The cyclic mechanism (with their Hamilton-Standard equipment) occurred at a rate of ~150 cycles/s as an equilibrium process.

Subsequent R&D work[10] utilized the X-ray camera to provide signals to generate a feedback actuation to control the weld beam current to effectively suppress spiking in partial-penetration welds for work done with aluminum alloys. Feedback techniques to suppress spiking, however, appeared to increase the tendency toward cold shut formation.

4.4 ORNL Electron-Beam Welding Experimentation for Flawing Applications

Our EB welding work for flawing applications can be summarized in three separate categories: (1) welding of flaws on outside surface of cylinder, (2) welding of restricted-access flaws on inside surface of cylinder (right-angle beam transmissions), and (3) welding of full-access flaws on inside surface of cylinder. Flaw depth and thus EB weld penetration requirements varied for the three categories: 8 to 10 mm ($^5/_{16}$ to ⅜ in.) for the outside-surface flaws (maximum attainable), 6.5 mm (¼ in.) for restricted-access flaws, and 16 to 19 mm (⅝ to ¾ in.) for full-access inside-surface flaws.

4.1 Welding of flaws on outside surface of cylinder

Oak Ridge National Laboratory's (ORNL's) initial large-scale EB experimentation efforts started 1974 for an HSST Program vessel requiring the development of autogenous welds that cracked o[illegible]ogen charging to yield sharp flaws of known geometry. We concentrated on developing parameters for producing welds 8 to 10 mm ($^5/_{16}$ to ⅜ in.) deep within premachined trapezoidal cutouts 25 mm (1 in.) wide by 457 mm (18 in.) long by 127 mm (5 in.) deep (Fig. 21) on the exterior surface of 152-mm (6-in.) wall thickness pressure vessels[11-13] of A533, Grade B, Class 1 steel plate.

Our welding was performed in the then AEC-owned 2.7 × 1.6 × 2.3 m (108 × 62 × 92 in.) model VX Sciaky weld chamber in Oak Ridge. The floor of the chamber required the addition of load-distributing beams to properly support the 7.6-t (8⅓-ton) vessel (less head) without buckling. A special dual beam track carrier and skid rail tracks were built to transfer the vessel in and out of the chamber. Figures 22 and 23 show the vessel entry into the chamber.

For the development program we selected a 156-mm (6⅛-in.) torch-to-work distance and a 40-kV welding voltage. Thus, the gun would ride ~25 mm (~1 in.) above the outside surface of the vessel. Initial trials were run on flat plates to find amenable combinations of current and speed ranges for welding the bottom flat portion of the trapezoid; a current range of 150 to 180 mA and a speed range of

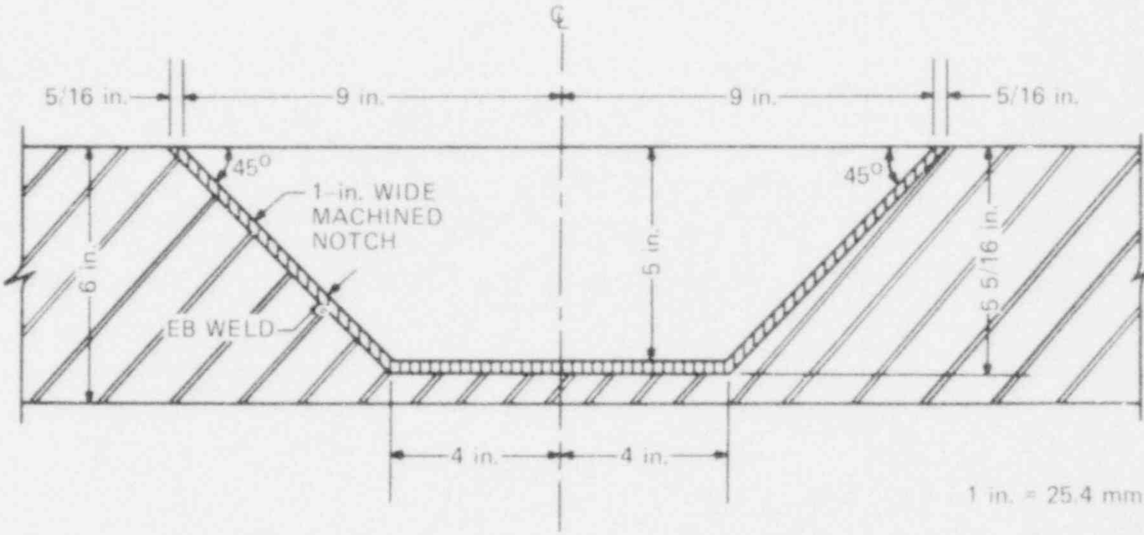

Fig. 21. Flaw design for HSST Program intermediate test vessel V-7 series.

2.0 to 2.3 m/min (80 to 90 in./min) were selected. Follow-up trials were then held on flat plates set at a 45° angle to simulate the trapezoidal side slopes. Integration of both horizontal and vertical torch travel at like speeds was determined to be necessary to obtain a resultant slope-surface welding speed about equal to the speed selected for the groove bottom. Trials on combination flat plates placed horizontally and at a 45° slope and tack welded at their junctions established techniques for overlapping welds at the bottom trapezoid corner. Welding must be uphill to keep the weld puddle behind the weld beam because gravity in downhill welding causes the puddle to advance into the weld arc. Therefore, the trapezoid had to be welded in two segments: a combined horizontal and uphill slant weld, and a second slant weld with minimum horizontal run to overlap the first weld near one trapezoid corner. A controlled overlap of 10 to 13 mm (⅜ to ½ in.) was necessary to maintain uniform weld depth when programming constant weld speed travel off the tungsten starter target at full welding current without using current upslope regulations. Lengthening the overlap works adversely; the resultant double-bead portion tends to blend metallurgically so that it no longer forms the tight bead-centered chill-line martensitic zone required for forming the crack on hydrogen charging.

Repeated trials were made on A533 materials 152 mm (6 in.) thick with a slot 25 mm wide by 127 mm deep (1 in. wide by 5 in. deep), as shown in the right view of Fig. 24, to check for weld beam distortion and beam attachment to the groove sides. Magnetic beam distortions were noted, especially where the slots were not balanced perfectly within the specimens or where the weld path was not well centered within the slot. Insertions of 0.1-mm-thick (5-mil) sheets of a soft-iron shielding material to cover the sides of the grooves to reduce or negate the effects of uneven magnetic distributions within the A533 work materials proved to be of little value. Handling and attachment difficulties prevailed and produced new problems, including frequent weld contamination where liners overheated or slipped. However, gaussmeter checks of a final prototype block (Fig. 24, left view) and of vessel V-7 indicated fairly even magnetic field distributions for both units. The decision was made to purposely offset the weld bead in the prototype ±1.6 mm (1/16 in.) off the true centerline of the slot by rotating the specimen about its longitudinal center. The resultant weld "pulled" no more than 4 mm (5/32 in.) from its actual

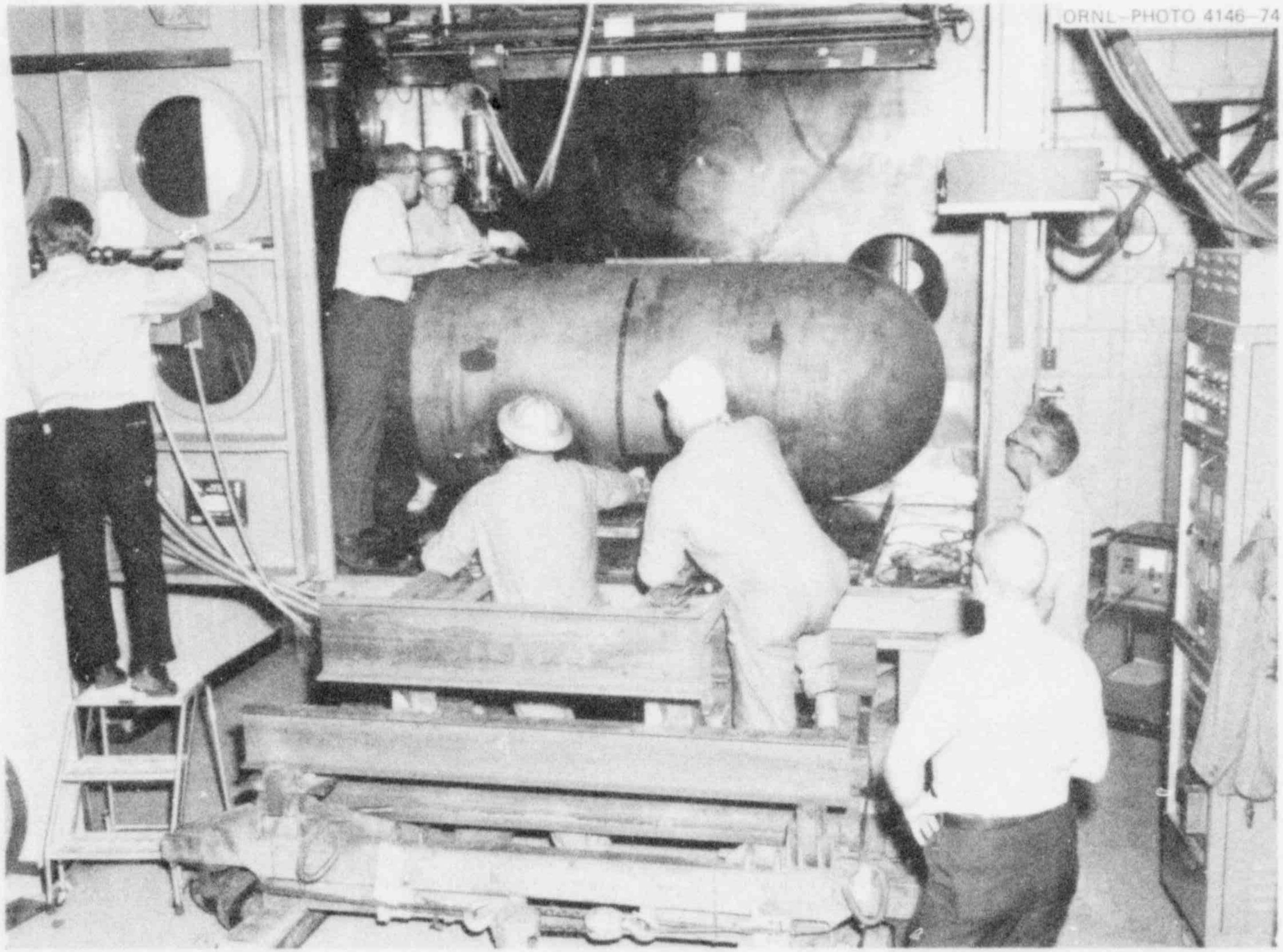

Fig. 22. View of vessel V-7 placement into Sciaky weld chamber.

ORNL–PHOTO 4150–74

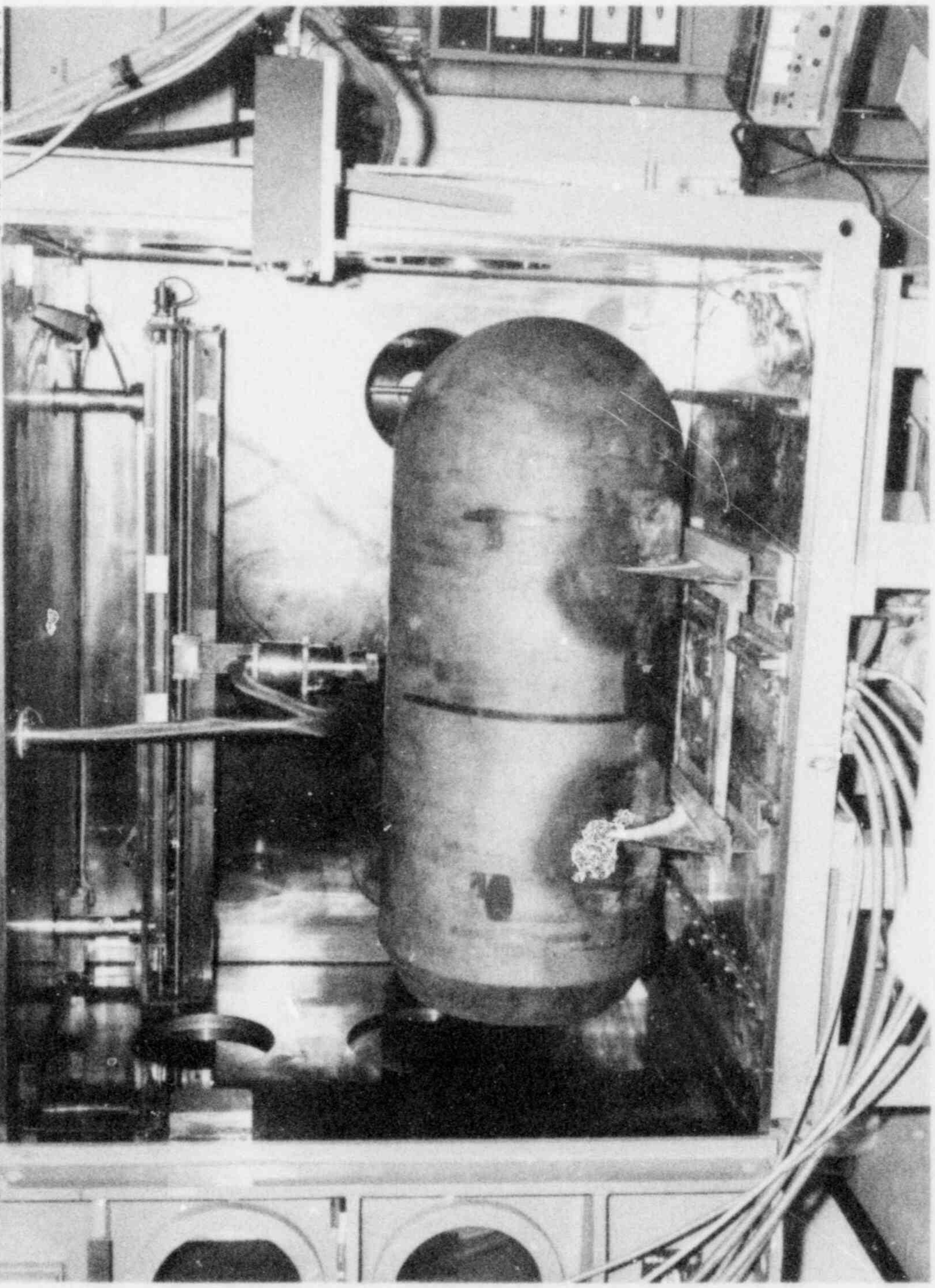

Fig. 23. View of vessel V-7 within weld chamber.

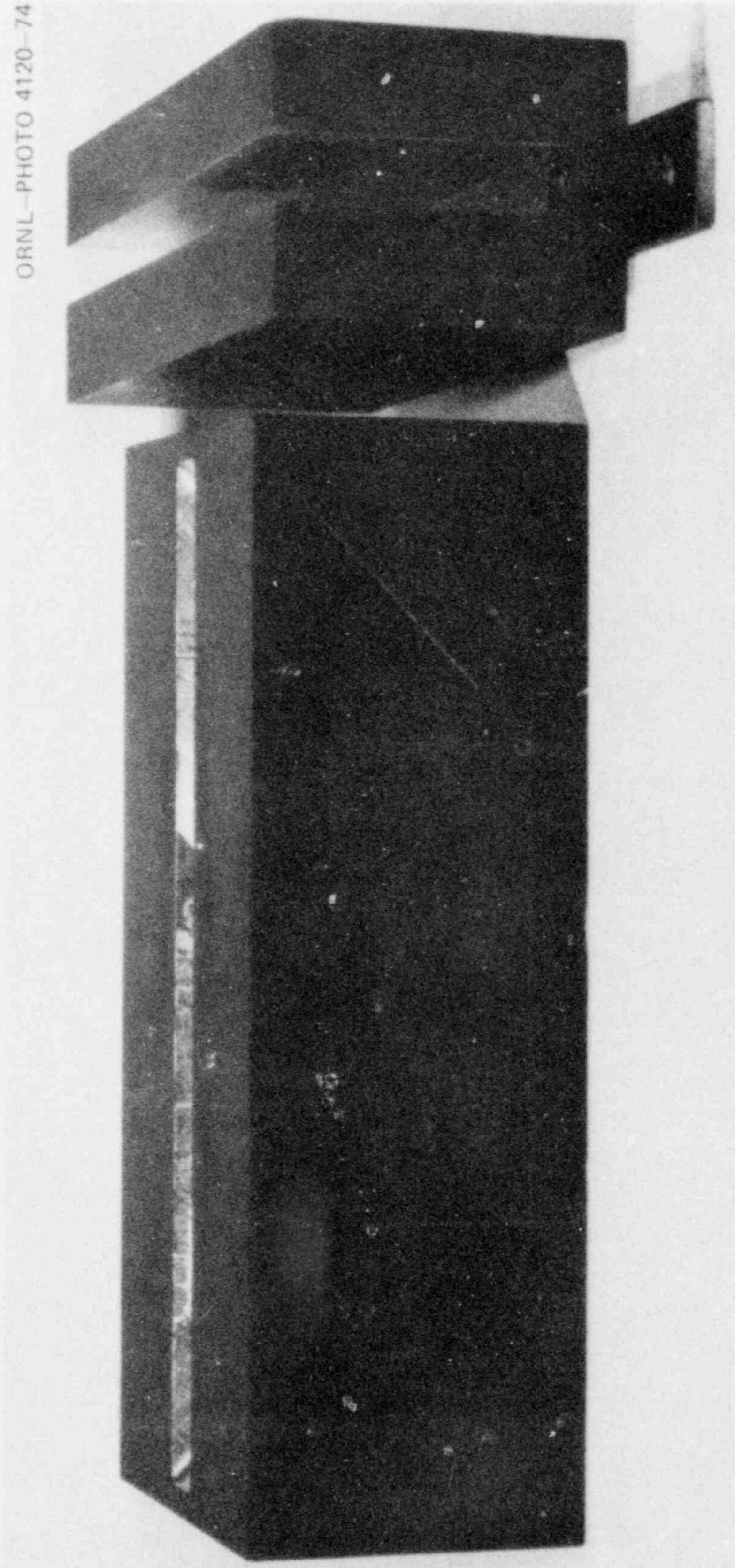

Fig. 24. Prototype blocks for practice flawing of vessel V-7 series EB welds by hydrogen charging.

centerline. The V-7 weld slot actually was centered somewhat better; the autogenous bead in V-7 deviated less than 3 mm (⅛ in.) from the true centerline. The welding parameters for the vessel weld are listed in Table 1.

Table 1. EB welding parameters for vessel V-7 series trapezoidal outside surface flawing welds

Material	Rolled steel plate, A533, Grade B, Class 1
Gun-to-work distance, mm (in.)	156 (6⅛)
Gun beam power, kV	40
Gun beam power, mA	120/185 (180 on horizontal; 185 on slopes)
Weld travel speed, m/min (in./min)	2.3 (90)
Energy density, J/min (J/in.)	189 to 194 (4800 to 4933)
Focal current setting	Milliamperes required for "sharp" + 4 mA, equivalent to 427 mA with "sharp" located 3 mm (⅛ in.) above work surface
Chamber vacuum, Pa (torr)	$<0.67 \times 10^{-3}$ (5×10^{-6})
Average bead	Pear shaped, 3-mm (⅛-in.) top surface width × 8-mm (5/16-in.) penetration.

Identical trapezoidal flaw preparations and EB welds were used for the two retests of vessel V-7, the V-7A and V-7B tests. For these tests we first removed the flawed areas from the previous test and then plugged the cutouts to American Society of Mechanical Engineers (ASME) Code Section XI half-bead repair (stick electrode) procedures.[12,13] The V-7A test flaw was placed longitudinally centered into the cylindrical portion of the vessel, spaced 135° away from the plug repair. The V-7B flaw was placed similarly, with the flaw located within the HAZ of the half-bead weld repair of the V-7A test. The purpose of the V-7A test was to compare the mode and effects of crack propagation for sustained-loading pneumatic vs hydrostatic tests. The V-7B test was conducted to test half-bead weld repair effectiveness and obtain crack propagation comparisons for flaws within and outside of postweld heat-treated stress-relieved materials. For all tests, EB welding parameters were as listed in Table 1.

The half-bead weld repairs, however, had some effect on the magnetic behavior of the vessel. In the machined notch of vessel V-7A, a high magnetic flux density [up to 6×10^{-3} T (60 G)] was encountered. This condition had not been experienced in vessel V-7 preparations, for which flux densities were about 3×10^{-4} T (3 G). The polarity (negative ground) of the dc arc welding electrode and the location of the attachment of the ground during half-bead repair welding are believed to account for the magnetization observed.

Electron-beam welding experiments on magnetized prototype test pieces had provided earlier indications that high and nonuniform magnetic flux density in the notch to be welded would cause significant deflection of the EB. Under such conditions, the deflected beam is not normal to the bottom surface of the groove. Severe transverse beam deflection can also cause attachment of the beam to the side wall of the machined groove. A longitudinally deflected beam also may lose sharp focus, which adversely affects depth of penetration. Earlier experimentation had indicated beam distortion problems with magnetic flux densities of 5×10^{-4} T (5 G) or more.

Many attempts were made to degauss the vessel and reduce the residual magnetic field before the vessel was placed into the weld chamber. Both ac and dc degaussing procedures were used. Results with direct current were highly unpredictable; flux increases were noted on some occasions. Effective degaussing was achieved by wrapping a 150-m (500-ft) No. 2 weld cable in continuous coils in three perpendicular planes about the vessel. Alternating current voltages were applied to generate up to 250 A. Magnetic flux densities in the vicinity of the vessel slot were reduced to 25% of initial values, or to about 15×10^{-4} T (15 G) maximum and about 8×10^{-4} T (8 G) average. Thereafter, two 0.1-T (1000-G) permamagnets were used effectively during EB welding for flux trimming so as to keep the weld beam centered along the longitudinal axis of the notch.

Practice trials on a series of blocks indicated that the EB bead positioning can be controlled precisely in fields up to 3×10^{-4} T. Gaussmeter checks within the notch of vessel V-7B again revealed nonuniform magnetic flux densities, with the highest readings 8×10^{-4} T (8 G) longitudinally and 5×10^{-4} T (5 G) transversely. These readings were about one-tenth the magnitude of the magnetic flux densities encountered with the V-7A repair weld. The improvement in the residual magnetism may have been the result of the planned symmetrical grounding connections used in the V-7B repair. Both of the electrical grounding connections were located 90° from the cavity along its transverse centerline. An arbitrarily located single ground had been used previously for the V-7A repair.

A prime requirement for the vessel V-7B test entailed the precise placement of the flaw weld into the center portion of the HAZ of the half-bead weld repair. The width of this HAZ is only about 2 mm (0.080 in.). Accordingly, special development was required to (1) properly index the repair weld's border for machining the trapezoidal notch well centered about the HAZ along the repair's longitudinal edge and (2) define the acceptable magnetic limits for achieving a weld bead for flawing within a zone ±0.4 mm (0.015 in.) of the HAZ's center.

Two ceramic 0.1-T (1000-G) magnets were machined by electrical discharge to fit within the trapezoidal notch. These magnets permitted flux trimming by varying orientations and locations so as to reduce and even the flux distribution along the EB traverse. By this means, the magnetic flux densities for vessel V-7B were held to a maximum of 2.6×10^{-4} T (2.6 G) before EB welding.

Actual forming of the EB weld in the notch had to be done in three separate steps: first along the deepest segment of the trapezoidal notch and then an upward pass along each slope. Tungsten target blocks were used to segment the overall weld. Gaussmeter checks made after each segment was welded indicated changes in magnetic flux patterns within the notch. Adjustment of the ceramic magnets, however, restored flux levels within the unwelded portions to levels $\leq 2.6 \times 10^{-4}$ T (2.6 G) before continuation of welding. The resulting EB weld was aligned properly within the required narrow band spanning the HAZ's center.

4.4.2 Welding of restricted-access flaws on inside surface of cylinder: Right-angle beam transmissions

Flaws on the inside surface of A508, Class 2 steel cylinders were required in early 1975 for thermal shock tests on vessel cylinders. The requirements were for two types of ~6.5-mm-deep (~¼-in.) sharp crack fronts located axially within cylinders 533 × 241 × 914 mm (21 × 9.5 × 36 in.) long. Requirements were for invert flaws the total length of the cylinder within premachined keyway-type slots, and for semicircular inside flaws with a radius of ~19 mm (~¾ in.), as shown in Fig. 25 (ref. 14). The extreme space confines of a 241-mm-diam (9.5-in.) cylinder passage called for the development of a special right-angle beam bender to permit the 165-mm-diam (6.5-in.) Sciaky weld gun to travel axially through the passage and produce a weld perpendicular to the normal straight weld direction. The bender shown in Fig. 26 was developed jointly by Sciaky Brothers, Chicago, Illinois, and ORNL; was built by Sciaky; and used a special magnetic mirror coil for weld beam transfer to the perpendicular plane.

ORNL–PHOTO 4389–75

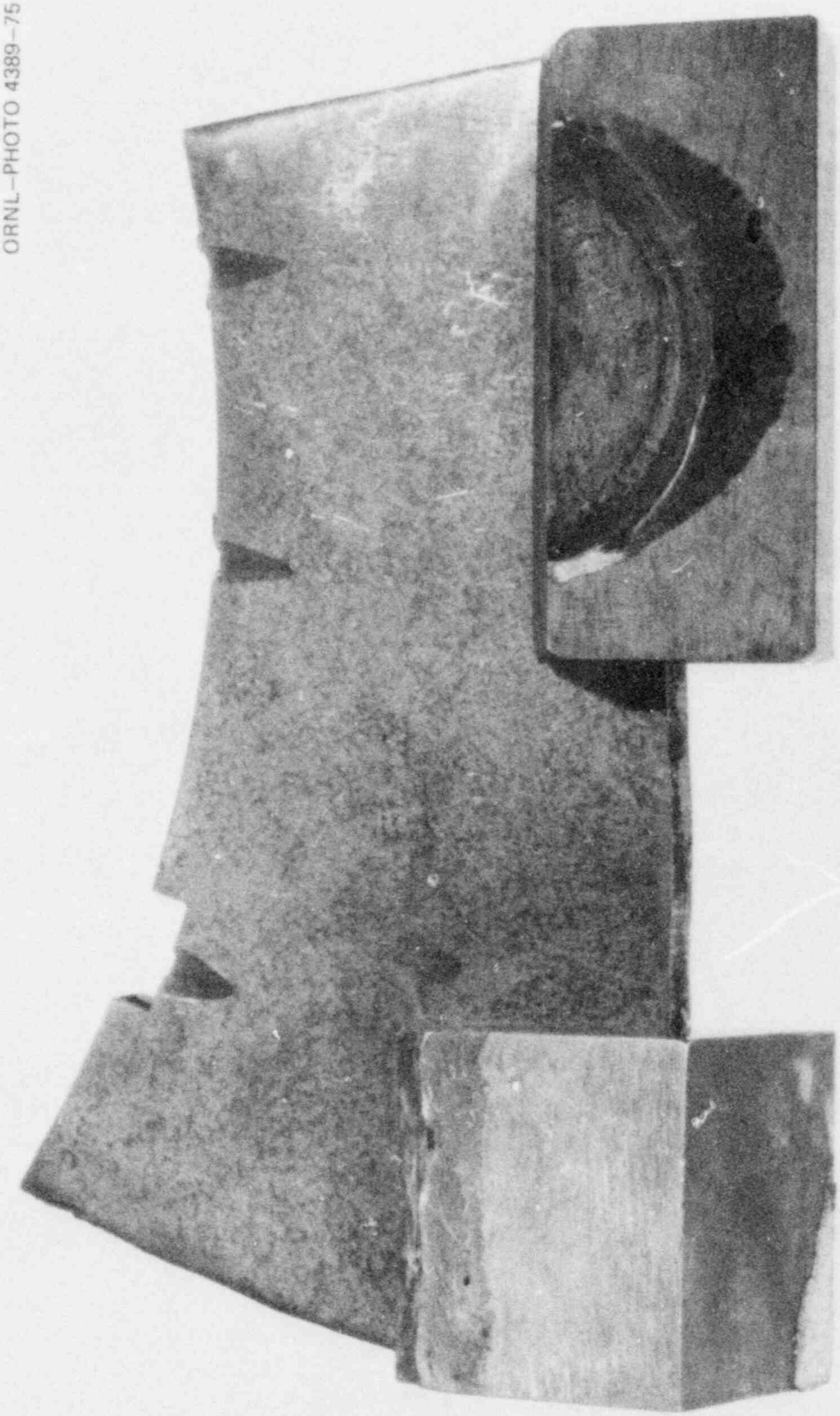

Fig. 25. Keyway and semicircular cylinder insert flaw specimens.

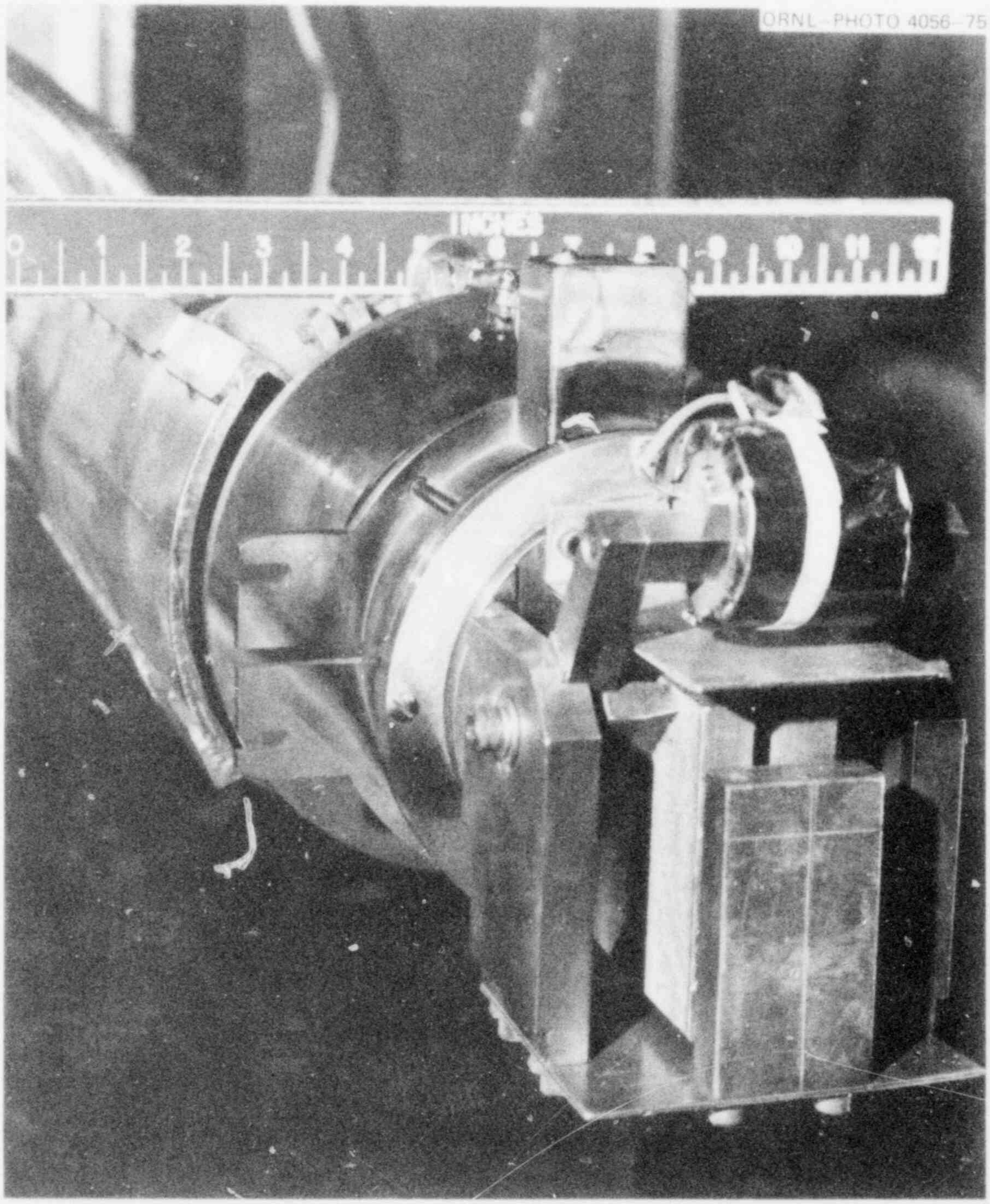

Fig. 26. Front elevation view of magnetic mirror coil beam bender mounted to EB gun.

Past EB work may be separated into two basic categories: conventional (along the axis of gun exit) welding and right-angle transmission (perpendicular to gun exit) welding. Distinct differences exist between the two welding modes, caused primarily by difficulties in beam focusing, gravity effects on the deflection coil mirror beam transmission, and concurrent beam efficiency losses.

The bent beam does not focus to the sharp point common in routine EB gun operation; the bent-beam focus might be said to be a series of overlapping points or an extremely short line, which exhibits sharp focus characteristics within the direction of the line only. Present equipment permits only axial EB welding; the linear focus characteristic does not allow welding in a transverse mode. Likewise, linear focus characteristics require that the exciting beam operating the "mirror," powered by separate integrated power supplies, be in the direction of gravity to attain consistent and uniform bead shapes.

The illustrated EB gun mounting (Figs. 27 and 28) traveling through a practice setup pipe parallel to and in the horizontal plane of the pipe proved to be an adequate arrangement for placing later autogenous welds to flaw the thermal shock cylinders. Maximum bead penetrations (flaw depths) attainable with the deflection coil attached to the weld gun were about 6.3 mm (¼ in.), with the gun operated near the maximum 50-kV, 185-mA rating of bend coil component parts. Typical resultant bead contours, after hydrogen-charge cracking, are shown in Fig. 29. Procedural development work also required special tungsten target block exit and entry angulation to accommodate the line rather than the point focus beam. Tack welds were used to anchor the starter and finish blocks within the cylinder (Fig. 30). The installation of cylinders in the weld chamber is displayed in Fig. 31. Typical parameters for bent-beam welds in thermal shock cylinders are listed in Table 2.

Table 2. EB welding parameters for deflection-coil (right-angle) flaw welding for thermal shock test cylinders

Material	Forged steel plate, A508, Class 2 [(material quench only, from 871°C (1600°F)]
Gun-to-work distance, mm (in.)	119 ($4^{11}/_{16}$) (torch or mirror axis to work dimension)
Gun beam power, kV	50
Gun beam power, mA	180
Weld travel speed, m/min (in./min)	2.0 (80)
Energy density, J/mm (J/in.)	266 (6750)
Focal current setting	Milliamperes required for "sharp," equivalent to 505 mA with "sharp" located at bottom surface of keyway trough or half-depth of half-moon; see drawings below
Chamber vacuum, Pa (torr)	$<0.67 \times 10^{-3}$ (5×10^{-6})
Average bead	Pear shaped, 3-mm (⅛-in.) top surface width by 6.4-mm (¼-in.) penetration

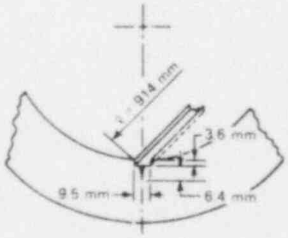

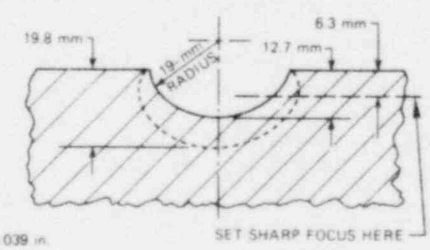

1 mm = 0.039 in.

KEYWAY SLOT FLAW WELD
END ELEVATION

HALF-MOON CIRCULAR FLAW WELD
CENTER SECTION

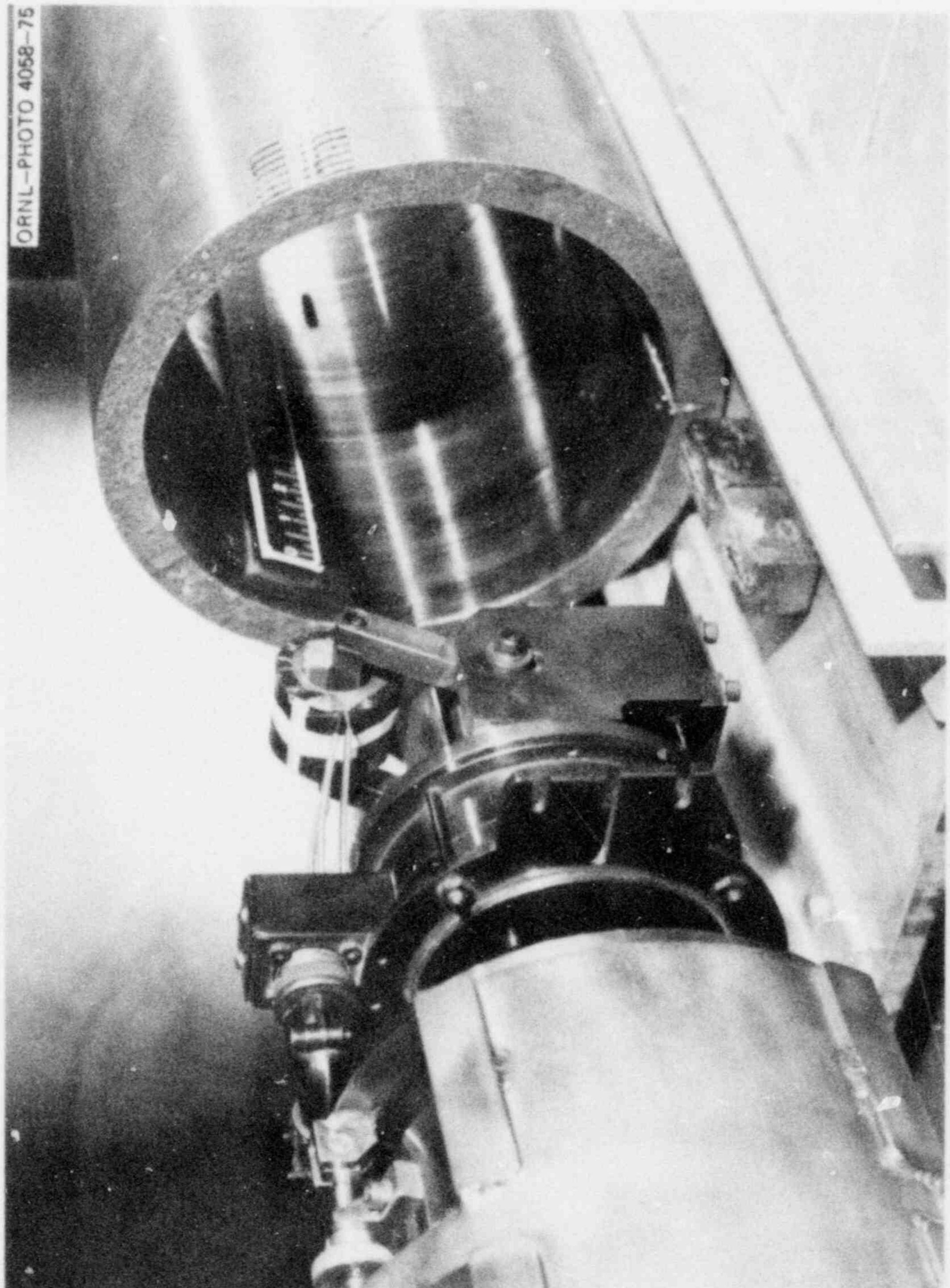

Fig. 27. Side elevation view of EB gun–beam bender assembly entering pipe.

ORNL–PHOTO 4055–75

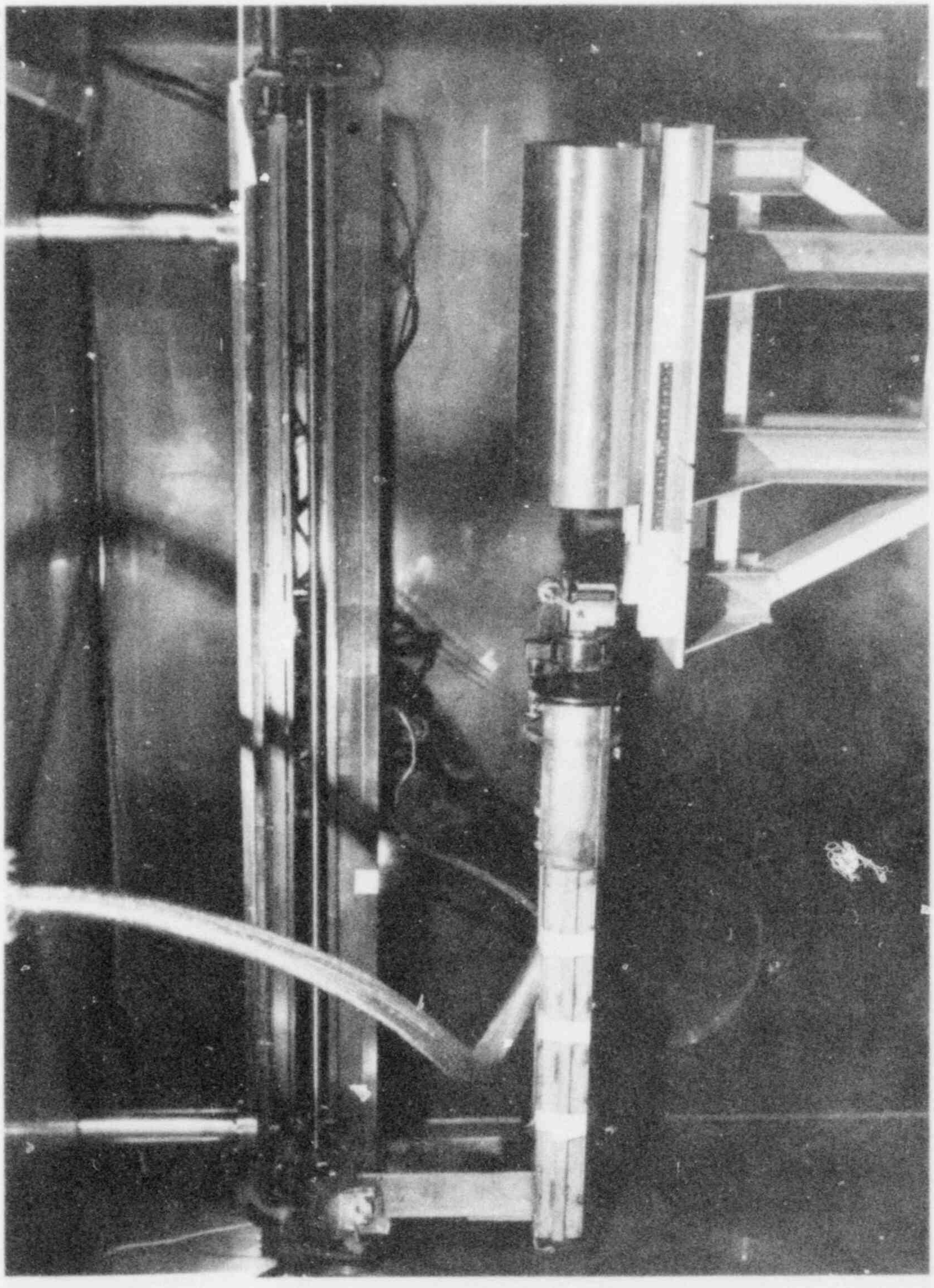

Fig. 28. Overall view of beam-bender EB gun assembly prior to pipe entry.

ORNL–PHOTO 4054–75

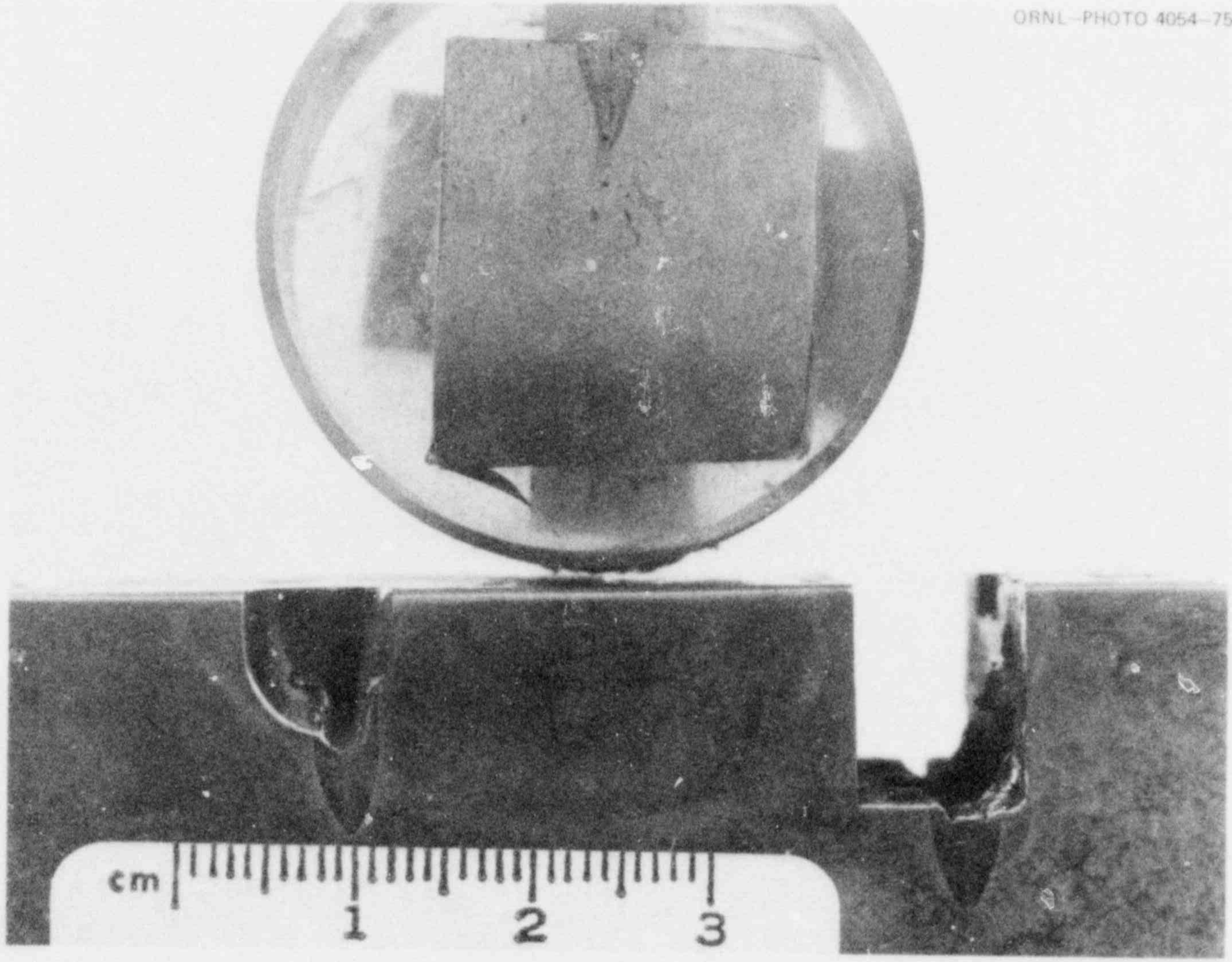

Fig. 29. Bead contour for right-angle beam transmission EB welds on pipe interiors.

ORNL–PHOTO 4057–75

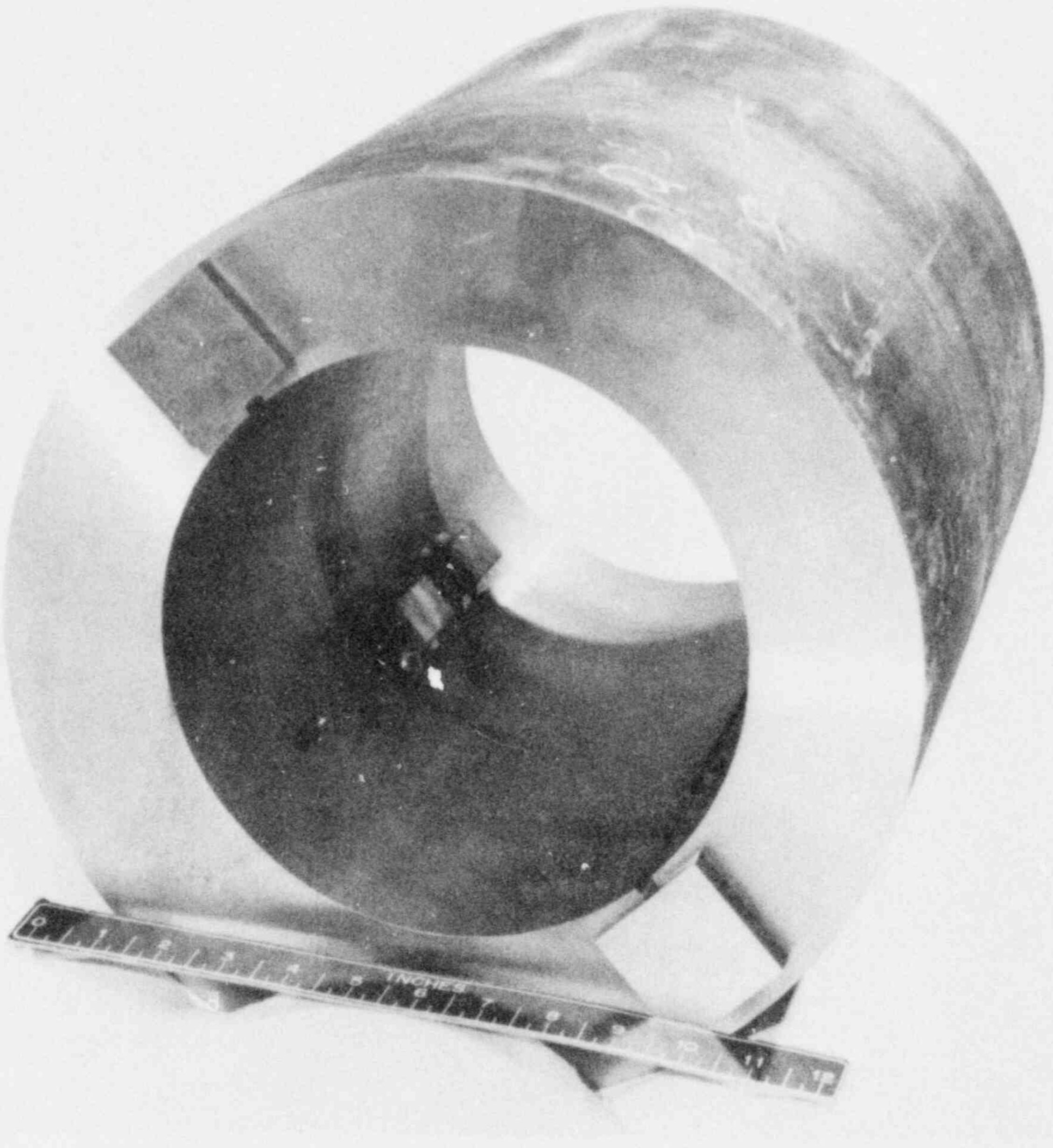

Fig. 30. View of EB weld setup, including target placement for inside-surface semicircular flaw welds.

A noteworthy observation: nearly all of the EB welds placed onto the A508, Class 2 practice and test unit stock at the fast welding speeds of 2000 to 2300 mm/min (80 to 90 in./min) would crack during the postweld cooldown. The AE monitoring setup shown in Fig. 32 employed several steel-bailing-wire wave guide transmissions from the specimen, via sensors mounted to the exterior of a penetration cover, which was attached on the weld box vacuum chamber side to a Trodyne monitoring system. The monitor identifies AE pulses from the cracking and determines the time of occurrence of the crack. Elapsed average time delays of about 23 s after a weld start to the occurrence of a significant AE burst seemed to indicate weld bead advance of ~875 mm (~34 in.), or nearly through the actual cylinder

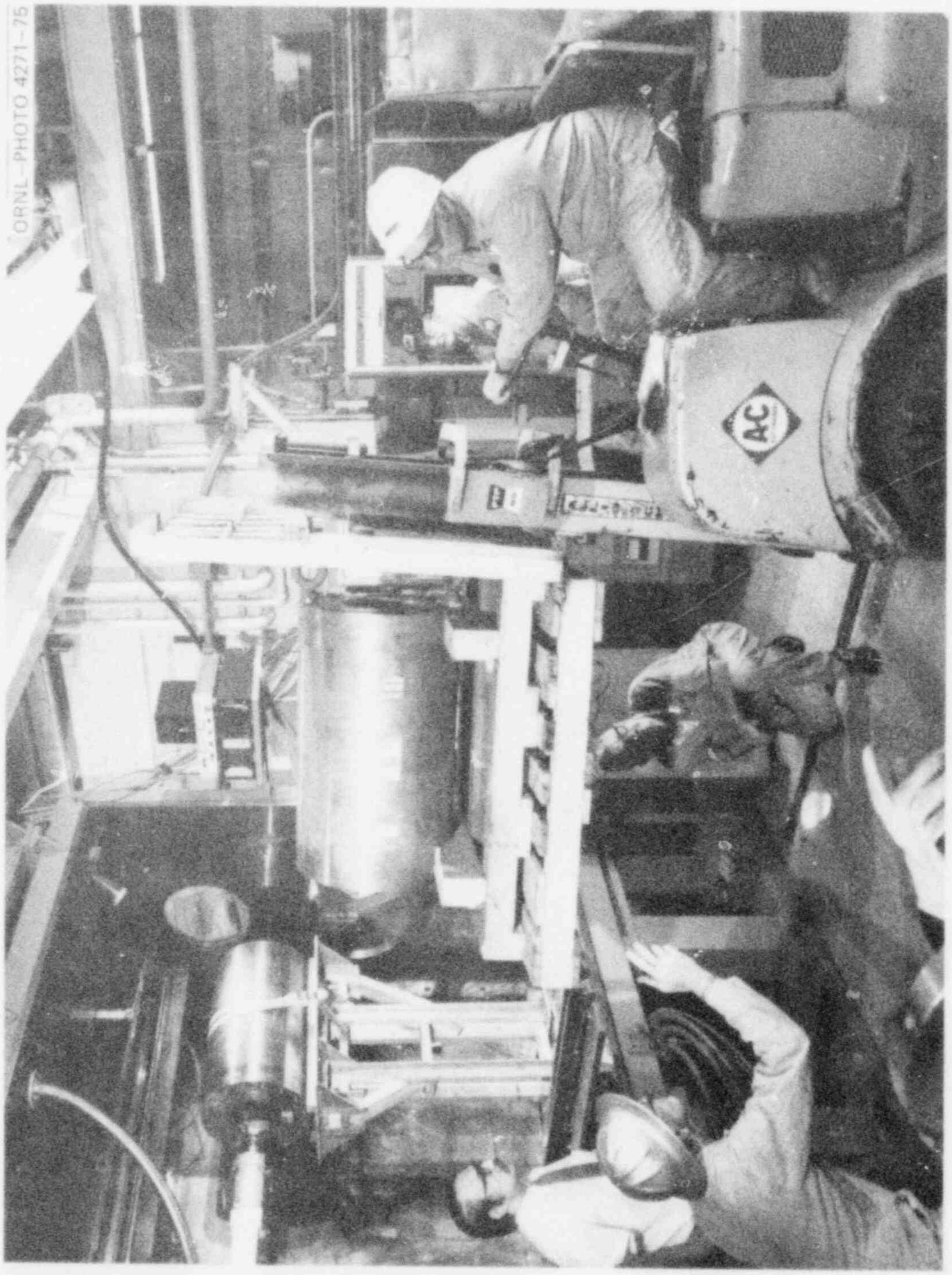

Fig. 31. View of thermal shock weld cylinder placement into weld chamber.

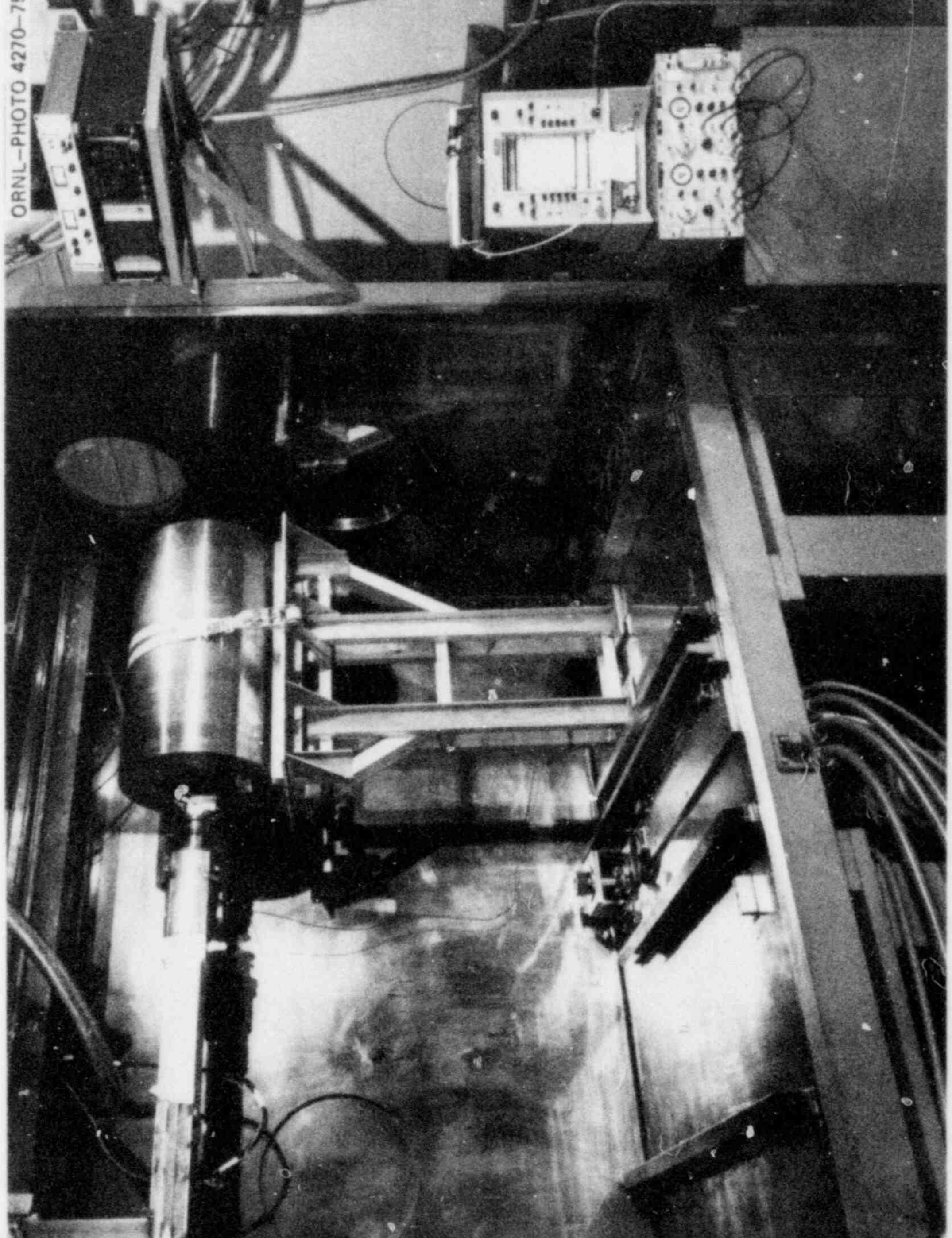

Fig. 32. View of thermal shock vessel TSV-1 within weld chamber.

length, for the invert welds prior to pop-in cracking of the bead, and an ~22-s delay in crack start beyond weld completion for the semicircular welds.

The A508, Class 2 thermal shock cylinder material used in the first four experiments, TSE-1 through TSE-4, was in the quenched-only [from 871°C (1600°F)] condition, thus leaving it in a considerably more brittle state than tempered steel. The cylinders represented center forging stock originating from treepans of Shell Nos. 7, 8, and 9 of National Forge, Erie, Pennsylvania, heats 3V924 and IV 3828, for intermediate test vessels V-3, V-4, and V-6 (ref. 15). Center forging material, which contains most of a melt's impurities, is usually quite cruddy. Ladle chemistry data indicated carbon content at 0.25, manganese at 0.86, and silicon at 0.35 for a carbon equivalent of about 0.55.

Posttest metallographic examinations of the cracked weld and crack propagation revealed that the propagating crack appeared to follow manganese sulfide inclusions in the steel.[16,17] Hardness checks also revealed considerable scatter in values and streaks of elevated hardness peaks. We have no precise conclusion for what started pop-in cracking of the EB bead during cooldown without the need for subsequent hydrogen charging. Inhomogeneities and dirt inclusions within the center forging treepan material are most likely the prime factors.

4.4.3 Welding of full-access flaws on inside surface of cylinder

The requirement for internal welding on cylinders with inside diameters large enough to permit conventional EB gun positioning and operation, without need for beam-bending devices, was for the introduction of 16-mm-deep (⅝-in.) continuous axial flaws to the internal surface of 991-mm-OD × 686-mm-ID × 1219-mm-long (39-in. × 27-in. × 48-in.) vessel cylinders.[18,19] These welds, after hydrogen charging, serve to provide the flaws for our thermal shock test work for thick-walled sections of A508, Class 2 steel tempered at 600 to 650°C (1115 to 1200°F). The thermal shock is administered by submerging the test specimen, uniformly preheated to 93°C (205°F), in liquid nitrogen at −196°C (−320°F).

Optimum EB welder output was tried for initial development trials on steel plate stock to find the maximum penetration attainable with our equipment. We eliminated the 500-mA capacity gun, which forms too wide a beam, producing an excessively wide bead with a ball-shaped contour. Such beads are not amenable to hydrogen-charge cracking. Near maximum output from the smaller 250-mA capacity gun (55 kV and 225 mA) produced autogenous beads averaging 19 mm (¾ in.) deep, with the proper masonry-nail-shaped contour amenable to cracking. These welds, however, were full of voids and exhibited irregular, highly spiked bottom profiles, with spiked bottom portion depth variations of 3 mm (⅛ in.) to ~6.5 mm (~¼ in.).

Consideration was given to the attempt to suppress spiking for the deep penetration welds required for our flawing applications. Feedback and beam penetration controlling were investigated.

Our 30-kW Sciaky welder is one of the first high-power machines built and hence does not contain today's state-of-the-art fast-response electronic circuitry. Correction capability via instantaneous signal feedback is not available. There are also physical space limitations within our chamber to mount an X-ray camera for the 1.22-m-long (4-ft) welds for cylinder inverts. The 2.74-m-long (9-ft) chamber leaves but 0.3 m (1 ft) total end clearance, which barely represents the minimum requirement for weld-gun-to-work entrance and exit positioning and gun support carriage frame upright space as shown in Fig. 33.

Extensive work by the Lawrence Radiation Laboratory, University of California, Livermore, California,[20] suggests that spiking is a function of beam power density and total beam power and can be

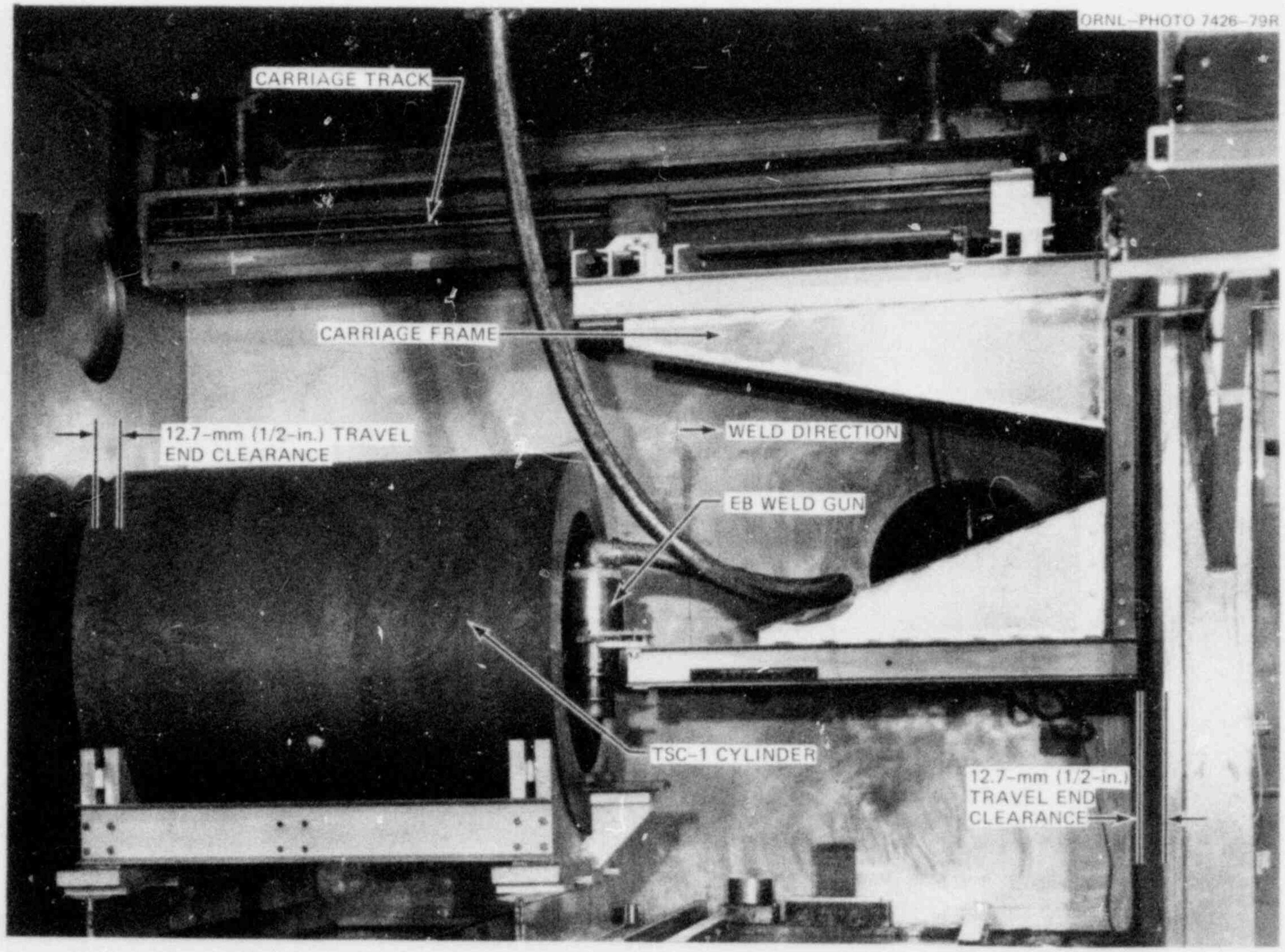

Fig. 33. View of thermal shock cylinder TSC-1 within weld chamber.

minimized by reducing penetration depth. The investigators studied the effect of five machine parameters — accelerating voltage, heat input, travel speed, beam focus position, and beam oscillation — on the amount of spiking in a deep partial-penetration EB weld. They noted that when the EB is operating in the "hole-drilling" mode, any parameter change that reduces the power density of the beam in the hole reduces spiking and gives a smoother root, but it also reduces the depth of penetration. When the power density of the beam is increased to regain the depth of penetration, the amount and length of spiking are increased. The investigators concluded, therefore, that spiking is not a function of individual machine parameters but is inherent in a high depth-to-width-ratio EB weld.

Based on the aforementioned, the decision was made to forego timely and expensive feedback corrective measures and concentrate primarily on "softening" the beam to reduce spike depth. The attempt was not to attain maximum possible weld penetration but to try instead to produce welds with the best depth penetration attainable with reduced spiking and fewest void formations. Flawing criteria were then to be adjusted to that penetration.

Void formations, also termed unfused areas or cold shuts, seem predominant in excessively spiked maximum-penetration welds. Void size, number, and even positioning (within the weld) are all directly proportional to the amount of spiking in an EB weld. In sharp-focus maximum-penetration welds, cold shuts appear to occur deep in the root area. These voids may be formed when molten metal following the beam fills the spike holes and freezes before the weld bonds to the sides of the hole. With the softened or defocused beam, cold shuts appear to increase in size and decrease in number, but they also tend to form above the root, extending up on the sides of the fusion zone.

We defocused the weld beam by shifting "sharp focus" to occur above the work to reduce spiking and to "elevate" cold shut voids from the root of the bead (the zone that provides us, upon hydrogen charging, with the sharp crack front) to an elevated zone bottoming somewhere between 1.5 mm (1/16 in.) and 5 mm (3/16 in.) above the root. "Sharp" weld beam focus is at the focal distance for the optimum depth narrowest nail-shaped bead cross section for a given EB gun-to-work setting and preselected beam accelerating potential. Focusing current settings are determined for sharp focus by visually observing the size and brilliance of the spot where all weld beam rays intersect the top surface of the work while operating the EB gun at full preselected weld voltage and nominal current, usually from 20 to 30 mA. For our defocused beam work, sharp focus was then reset to occur between 6.5 and 9.5 mm (¼ to ⅜ in.) above the work surface, resulting in sharp + 8 to sharp + 12 mA focal current settings.

It is also possible to operate the weld gun with the beam focused into the work or with "sharp (−)" focal currents. The negative focusing below the steel surface, however, tends to cause coarse, nonuniform bead top contour, with frequent lack of fusion for the upper portions of the bead sidewalls. These welds, upon hydrogen charging, form cracks that do not follow the entire martensitic chill line along the bead center but tend to branch to form cracks along one or both sides of the bead. Branching usually occurs at the locations of void pockets.

Flawing welds for thermal shock experiment TSE-5 were performed successfully on prolongation cylinder TSP-1 and test cylinder TSC-1 using the welding parameters listed in Table 3. The open-ended test cylinders appeared magnetically balanced, with no beam deflection problems due to magnetic effects noted during welding.[19,21]

Table 3. EB welding parameters for welding of full-access deep inside-surface flaws in thermal shock test cylinders

Material	A508, Class 2 forged steel cylinders
Gun-to-work distance, mm (in.)	146 (5¾)
Gun beam power, kV	55.25
Gun beam power, mA	218 to 220
Weld travel speed, m/min (in./min)	2.12 (83½)
Energy density, J/mm (J/in.)	343 (8700)
Focal current	Milliamperes required for "sharp" + 8 mA, equivalent to 508 mA, with "sharp" located 6.5 mm (¼ in.) above work surface
Vacuum chamber, Pa (torr)	$<0.67 \times 10^{-3}$ (5×10^{-6})
Average bead	Masonry nail shaped; 2.3-mm (0.09-in.) top surface width × 16.5-mm (0.65-in.) penetration

REFERENCES

1. F. T. Witt, *HSST Program Semiannual Progress Report*, ORNL-4512, pp. 88–102 (Aug. 31, 1969).

2. J. G. Merkle, "An Analytical Basis for Notch Sharpening by Fatigue," ASME Paper 71-PVP-46 (May 1971).

3. R. W. Derby et al., *Test of 6-Inch-Thick Pressure Vessels. Series 1: Intermediate Test Vessels V-1 and V-2*, ORNL-8495, pp. 83–88 (February 1974).

4. R. H. Bryan et al., *Test of 6-Inch-Thick Pressure Vessels. Series 3: Intermediate Test Vessels V-8*, NUREG/CR-0675 (ORNL/NUREG-58) (December 1979).

5. P. P. Holz and S. W. Wismer, *Half-Bead (Temper) Repair Welding for Heavy-Section Steel Technology Vessels*, NUREG/CR-0113 (ORNL/NUREG/TM-177) (June 1978).

6. R. H. Bryan et al., *Test of 6-Inch-Thick Pressure Vessels. Series 2: Intermediate Test Vessels V-3, V-4, and V-6*, ORNL-5059 (November 1975).

7. D. A. Canonico and J. D. Hudson, "Technique for Generating Sharp Tracks in Low-Alloy High-Strength Steels," Paper 20 presented at the Fifth Annual HSST Information Meeting, Oak Ridge, Tenn., Mar. 25, 1971.

8. T. P. O'Brien et al., "Suppression of Spiking in Partial Penetration EB Welding with Feedback Control," *Weld. J.* **53**(8), 332-s (August 1974).

9. C. M. Weber, E. R. Funk, and R. C. McMaster, "Penetration Mechanism of Partial Penetration Electron Beam Welding," *Weld. J.* **51**(2), 90-s (February 1972).

10. P. Tews et al., "Electron Beam Welding Spike Suppression Using Feedb k Control," *Weld. J.* **55**(2), 52-s (February 1976).

11. J. G. Merkle et al., *Test of 6-Inch-Thick Pressure Vessels. Series 3: Intermediate Test Vessels V-7*, ORNL/NUREG-1 (August 1976).

12. R. H. Bryan et al., *Test of 6-Inch-Thick Pressure Vessels. Series 3: Intermediate Test Vessels V-7A Under Sustained Loading*, ORNL/NUREG-9 (February 1978).

13. R. H. Bryan et al., *Test of 6-Inch-Thick Pressure Vessels. Series 3: Intermediate Test Vessels V-7B*, NUREG/CR-0309 (ORNL/NUREG-38) (October 1978).

14. R. D. Cheverton and S. E. Bolt, *Pressure Vessel Fracture Studies Pertaining to a PWR LOCA-ECC Thermal Shock: Experiments TSE-3 and TSE-4 and Update of TSE-1 and TSE-2 Analysis*, ORNL/NUREG-22 (December 1977).

15. C. E. Childress, *Fabrication and Mechanical Test Data for Acceptance of the First Six 6-Inch-Thick Intermediate Test Vessels of the Heavy Section Steel Technology Program*, ORNL/TM-4351, pp. 18, 30 (October 1973).

16. R. D. Cheverton, *Pressure Vessel Fracture Studies Pertaining to a PWR LOCA-ECC Thermal Shock: Experiments TSE-1 and TSE-2*, ORNL/NUREG/TM-31, p. 197 (September 1976).

17. R. D. Cheverton and S. E. Bolt, *Pressure Vessel Fracture Studies Pertaining to a LOCA-ECC Thermal Shock: Experiments TSE-3 and TSE-4 and Update of TSE-1 and TSE-2 Analysis*, ORNL/NUREG-22 (December 1977).

18. G. D. Whitman and R. H. Bryan, *Heavy-Section Steel Technology Program Quarterly Progress Report for January–March 1979*, NUREG/CR-0818 (ORNL/NUREG/TM-324), pp. 90–99 (August 1979).

19. G. D. Whitman and R. H. Bryan, *Heavy-Section Steel Technology Program Quarterly Progress Report for April–June 1979*, NUREG/CR-0980 (ORNL/NUREG/TM-347), pp. 45–72 (October 1979).

20. R. E. Armstrong, "Control of Spiking in Partial Penetration Electron Beam Welds," *Weld. J.* **49**(8), 382-s (August 1970).

21. G. D. Whitman and R. H. Bryan, *Heavy-Section Steel Technology Program Quarterly Progress Report for July–September 1979*, NUREG/CR-1197 (ORNL/NUREG/TM-370) (April 1980).

Appendix

SYSTEM DESCRIPTION, PROCEDURES, AND OPERATING INSTRUCTIONS FOR SHARPENING SURFACE FLAWS BY FATIGUE, USING CYCLIC HYDRAULIC NOTCH PRESSURIZATION

A.1 INTRODUCTION

The main factors that affect the pressure generated in a machined notch are compressibility of the fluid, volume of the system, and displacement of the pump. Ideally, one would prefer a perfectly incompressible fluid and a "stiff" system of piping to minimize the size of the pump and the power required to generate high pressure. Lower compressibility also diminishes the amount of energy that is dissipated by the system as heat. For example, air is a highly compressible fluid; hence, if air is the working fluid in a "hydraulic system" and if one pump stroke reduces the total volume of the system to half its original volume, the pressure simply doubles. If, on the other hand, the working fluid is water, which is essentially incompressible, and if one pump stroke reduces the total volume to half the original volume, the pressure would be so high that the containment might rupture long before the total system volume was reduced to half. In practice, therefore, since both the fluid and the system are elastic, the peak pressure achieved can be adjusted by the selection of fluid type, total system volume, compliance of the system, and displacement of the pump. For a system of small enough volume and compliance, it is possible to attain the desired maximum pressure with a single pump stroke. With a fixed-displacement pump, adjusting system volume so that each pump stroke produces a pressure pulse of the desired magnitude is then practical. For systems of small volume, attempting to reach maximum pressure in one stroke is not practical. The compliance of gages and the presence of unwanted gas bubbles limit the amount of pressure that can be produced by a single stroke. Also, when the volume is necessarily large because of the size of the flaw, the compressibility of the fluid may be the limiting factor.

One pressure cycle may be accomplished by a single pump stroke if the conditions are consistent with the factors mentioned above. Otherwise, the pressure cycle must be accomplished by continued pumping to the desired pressure, at which time the fluid is relieved through a dump valve.

Leaks in the packing glands, valve seats, and other components and the temperature and viscosity of the working fluid also affect the performance of the system. Seats of valves or worn contact surfaces on valve stems may leak and thereby cause considerable difficulty in the control of system pressure. The effects of temperature on fluid properties must also be considered. The hydraulic fluid used should have relatively uniform compressibility and viscosity over the range of system operating temperatures encountered.

A.2 THE ORNL HIGH-PRESSURE HYDRAULIC PUMPING SYSTEM

A.2.1 Description of System and Components

Our high-pressure hydraulic system consists of a pump, a dump valve, a reservoir, a pressure gage, a variable-volume tubing leg, associated tubing, valves, and the specimen. Figure A.1 illustrates the setup schematically; Fig. A.2 is a photograph of an actual setup, including the ultrasonic inspection apparatus.

The pump is an air-driven, positive-displacement, differential piston pump with an output pressure capacity of 139 MPa (20,000 psi) when driven from a 0.69-MPa (100-psi) air supply. We use an

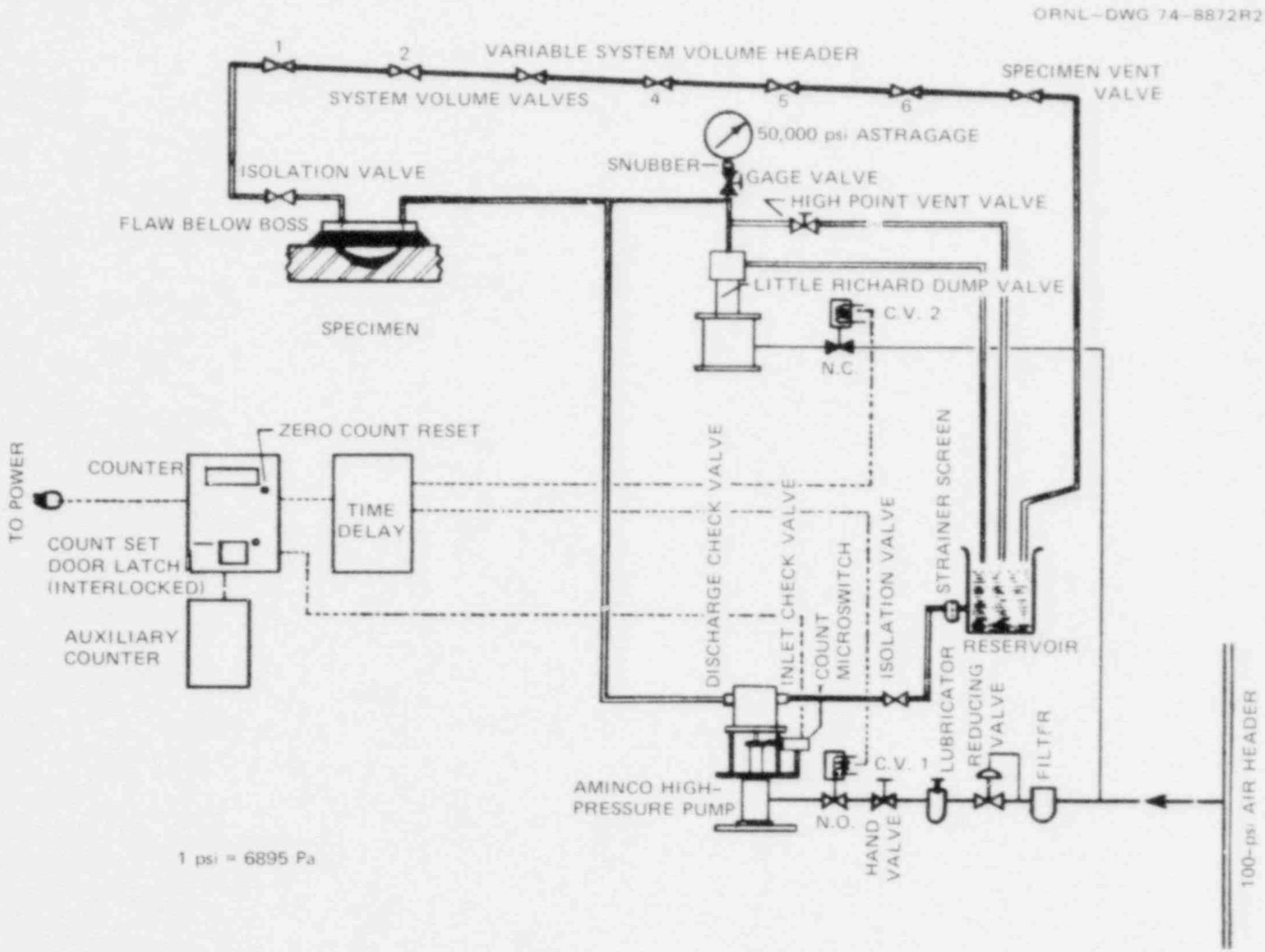

Fig. A.1. High-pressure hydraulic pumping system for pump-dump cycling for notch sharpening by fatigue.

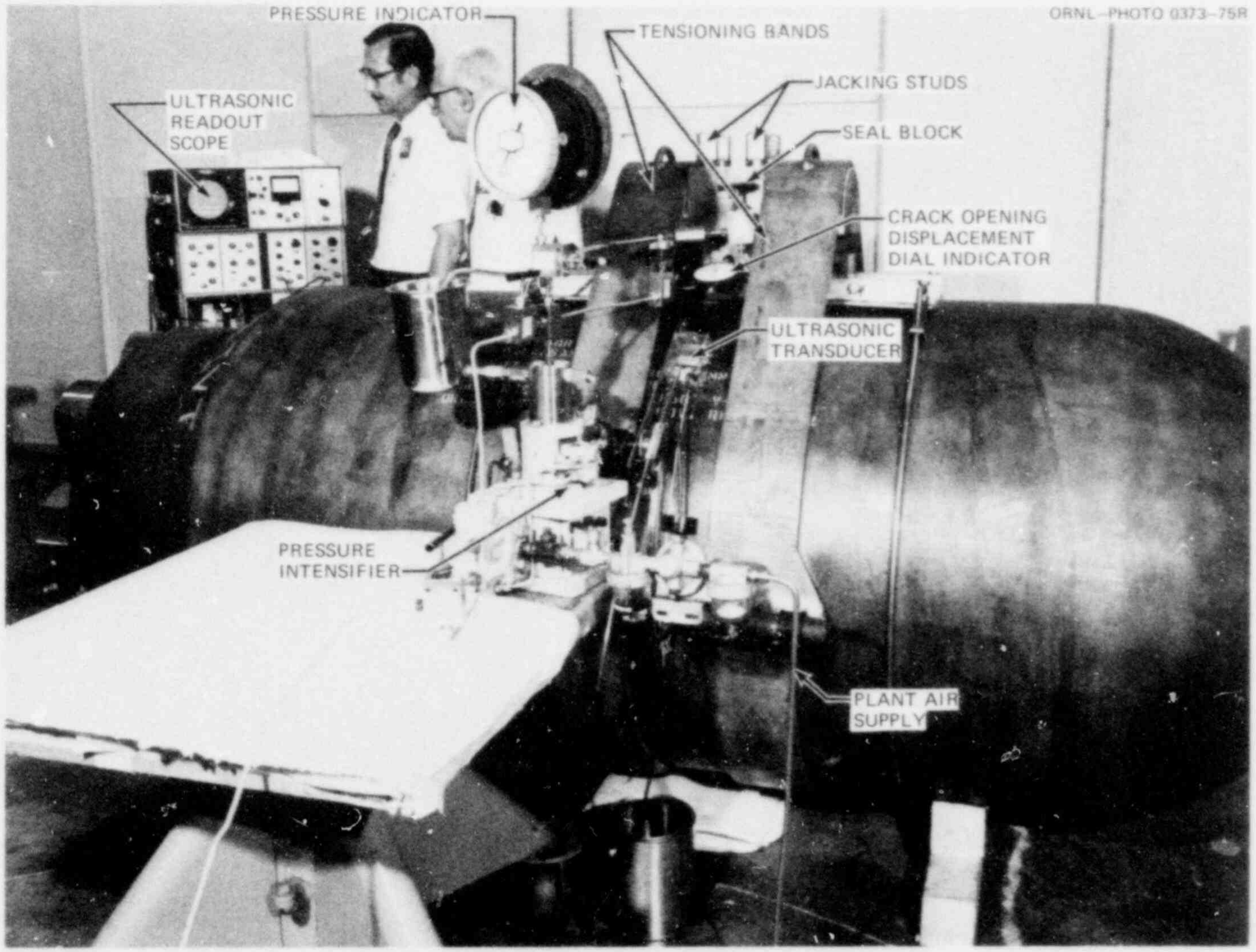

Fig. A.2. General view of crack-sharpening apparatus being used for an outside-surface flaw for an intermediate test vessel.

American Instrument Company single-ended model 46-13720 plunger pump. The dump valve is either an air-driven, positive-displacement, differential piston valve or a pneumatic, diaphragm-operated piston valve, as furnished respectively by the American Instrument Company [model 44-19730, 139-MPa (20,000-psi) "Little Richard" valve] or by the High Pressure Equipment Company [model SD-30, 207-MPa (30,000-psi) HIP "Remarco" valve]. The reservoir is a stainless steel 4-liter (1-gal) beaker, to which the feed lines are soldered. Screens are inserted into the line exit ports to filter the fluid. The pressure gage is a 345-MPa (50,000-psi) Astragage, which is accurate to ±5% of full scale. The variable-volume tubing leg consists of a series of high-pressure autoclave valves connected by short runs of tubing. The tubing is rated for 414-MPa (60,000-psi) service.

A.2.2 System Controls

The system for actuating the pump and the dump valve consists of a count switch, an electric counter, a time-delay relay, two solenoid valves, and an auxiliary counter.

The count switch is a microswitch that contacts a collar on the pump's plunger to count pump strokes (not pump cycles) to allow for coordination of suction and compression pump strokes with a preset count. It is designed to permit a fractional final pump stroke in order to actuate the dump circuit at a predetermined pressure. Fractional stroke adjustment is regulated by shifting the count switch up or down along the length of the plunger.

The counter accumulates the counts transmitted by the count switch and actuates an electric relay whenever the count reaches a number preset on the counter control. The counter is an ITT CE-62-BE-402 unit. Knurled wheels to preset the counter are located inside an interlocked door to prevent inadvertent changing of the preset adjustment. When the number of pump strokes reaches the preset level, the counter automatically resets itself and initiates the next cycle.

The function of the time-delay relay is to prolong the interval between the time that the pump reaches maximum pressure output and the time that the dump valve opens. On a large system, delayed action is necessary to allow the system pressure to peak before the dump valve opens to drop all pressure. The solenoid-controlled valves regulate the air supply to the pump and actuate the dump valve.

An auxiliary counter, which is wired to receive an electrical pulse from the signal that operates the solenoid on the dump valve, is used to count the actual cumulative hydraulic pulses, or cycles, to the specimen.

Additional information on specific system control details is discussed below.

A.3 OPERATING INSTRUCTIONS FOR THE ORNL HYDRAULIC PUMP-DUMP SYSTEM

A.3.1 Initial System Startup*

1. Fill the reservoir with No. 10 oil or with an oil-kerosene mixture.

2. Unplug the counter and control-box power-supply cords.

3. Open the reservoir isolation valve, the high-point vent valve, all valves on the variable-volume header, the specimen vent valve, and the gage valve.

4. Check the lubricator on the pump's air inlet for an adequate oil supply.

*Use diagram in Fig. 1 for reference.

5. Set the reducing valve on the pump's air supply to a low pressure, and then open the hand valve on the pump's air-supply line.

6. Adjust the reducing valve on the pump's air-supply line to supply air at a pressure of ~83 kPa (12 psig).

7. Gradually increase the air pressure to the pump until the pump's piston starts to operate.

8. Set the oil lubricator to deliver about one drop per minute.

9. Now run the pump until all air is out of the hydraulic system, and then increase the air pressure to the pump to speed up its operation after the lubricator is properly set.

   a. Close the high-point vent valve when all air is out of the system up to that point.

   b. Close the specimen vent valve and all variable-volume header valves when there is no more air in the reservoir.

10. With all valves closed, the system pressure should now start to build up. Observe pressure on the 345-MPa (50,000-psi) Astragage.

11. Now increase the air pressure to the pump to reach the desired system pressure for the specimen.

12. Open the door to the counter control and preset an estimated number of counts.

13. Close the door again and, using the white button, set the counter indicator to zero.

14. Energize the counter controller; plug in the supply cord.

15. Adjust the positioning of the count microswitch until the system begins to count for the desired pressure output. If the first pump stroke is not a downward or suction stroke, unplug the counter and replug it when the count and the stroke are in phase; that is, stroke 1—suction, stroke 2—compression, stroke 3—suction, stroke 4—compression, etc. The count microswitch can also be operated with a pencil to phase counts to strokes, but care must be exercised to prevent mashing one's finger.

16. The gage isolation valve should be shut off when the settings are being made for the desired pressure operation to protect the precision gage from chatter.

   a. The pump may stop when the gage isolation valve is secured because the total system volume is decreased with the gage volume removed. The actual air pressure required to operate the pump may exceed the pressure obtainable from the air supply. DO NOT INCREASE THE AIR PRESSURE TO THE PUMP AT THIS TIME. To compensate for the loss of gage volume and to enlarge the volume of the total system, either adjust the valves in parts of the variable-volume header (starting at valve 1) or move the count microswitch down along the pump's plunger attachment until the pump begins to run again. Both operations may be necessary.

   b. When the pump system pressure ratio has been adjusted, the pulse speed can be increased by increasing the air pressure to the pump. This speed may be increased further by adjusting (turning) the screw on the time-delay relay toward decrease.

17. During operation, continue to check the entire system for leaks. It does not take much of a leak to upset pressure output or system control. All leaks must be sealed at once, followed by readjustments as outlined above.

A.3.2 Restarts—For Pump Operation of a System That Is Already Set Up, with the Pump-to-System Pressure Ratio Previously Preset

1. Adjust count phase as described in items 14 and 15 of the previously detailed procedure.
2. Check oil supply reservoir; refill if necessary.
3. If in trouble, check the system pressure by unplugging the count controller and following the previously detailed procedure described in items 11 through 17.

A.3.3 Troubleshooting

The stem of the dump valve may wear (at a frequency of every 90,000 to 120,000 pump cycles) with repeated seating at pumping pressures in excess of 139 MPa (20,000 psig). The valve will then start to leak. If this should occur, refer to the American Instrument Company's manual on the "Little Richard" dump valve No. 44-19730 or No. 44-19731 for disassembly instructions and information on valve replacement parts.

The pump piston O-rings may wear and start to leak, or other pump problems may be suspected. If so, refer to the American Instrument Company's manual on air-operated piston pumps for liquid service No. 857B.

☆U.S. GOVERNMENT PRINTING OFFICE: 1980-640-245/082

NUREG/CR-1274
ORNL/NUREG/TM-369
Dist. Category RF

Internal Distribution

1. J. E. Batey
2. S. E. Bolt
3. C. E. Bolyard (Y-12)
4. R. H. Bryan
5. D. A. Canonico
6. W. F. Cartwright (Y-12)
7. R. D. Cheverton
8. J. M. Corum
9. G. M. Goodwin

10–14. P. P. Holz

15. R. A. Huber (Y-12)
16. J. D. Hudson
17. S. K. Iskander
18. T. A. King, Jr.
19. K. K. Klindt
20. J. G. Merkle
21. F. R. Mynatt
22. D. J. Naus
23. H. A. Pohto (Y-12)
24. J. L. Rich
25. G. C. Robinson
26. D. G. Scott (Y-12)
27. G. M. Slaughter
28. J. E. Smith
29. W. J. Stelzman
30. D. B. Trauger
31. H. E. Trammell
32. S. A. Wallace (Y-12)

33–37. G. D. Whitman

38. Patent Office

39–40. Central Research Library

41. Document Reference Section

42–43. Laboratory Records Department

44. Laboratory Records, RC

External Distribution

45. C. Z. Serpan, Jr., Reactor Safety Research, U.S. Nuclear Regulatory Commission, Washington, DC 20555
46. M. Vagins, Reactor Safety Research, U.S. Nuclear Regulatory Commission, Washington, DC 20555
47. Office of Assistant Manager, Energy Research and Development, DOE, ORO

48–49. Technical Information Center, DOE

50–459. Given distribution as shown in category RF (NTIS-10)